Resonance Raman spectra of highly oxidized metalloporphyrins and heme proteins*

Teizo Kitagawa and Yasuhisa Mizutani
Institute for Molecular Science, Okazaki National Research Institutes, Myodaiji, Okazaki 444 (Japan)

(Received 27 October 1993)

CONTENTS

* The authors would like to dedicate this paper to the late Professor Tatsuo Miyazawa who continuously encouraged them but who passed away during the writing of this paper.

Correspondence to: T. Kitagawa, Institute for Molecular Science, Okazaki National Research Institutes, Myodaiji, Okazaki, Japan.

0010-8545/94/$26.00
SSDI 0010-8545(94)01111-N

ABSTRACT

Studies of resonance Raman (RR) spectra of highly oxidized metalloporphyrins and heme proteins in the past decade are surveyed comprehensively. Following the introduction this article consists of two main sections. In Section 2 the Fe^{IV}=O stretching ($\nu(Fe^{IV}=O)$) vibrations of ferryloxo neutral and π cation radical porphyrins and their porphyrin in-plane modes are discussed and the characters of the Fe^{IV}=O bond and environmental effects on it are elucidated. For porphyrin π cation radicals, the RR spectral differences between the a_{1u} and a_{2u} radicals are interpreted in relation to the electronic properties of those orbitals for divalent metalloporphyrins as well as iron porphyrins. Some changes in vibrational characters on oxidation of the porphyrin ring are noted on the basis of isotopic substitution data. Studies of environmental effects on porphyrin π cation radicals permit one to deduce factors for determination of radical types. Current RR studies of nitrido iron and *N*-oxide iron porphyrins and other metal oxo porphyrins with M^{IV}, M^{V}, and M^{VI} ions are also covered. In Section 3 the present state of RR studies of reaction intermediates of heme enzymes containing ferryloxo neutral and π cation radical porphyrins is summarized, and discussion is focused on the $\nu(Fe^{IV}=O)$ RR bands. Attention is paid to compound I of horseradish peroxidase for which complete historical vicissitudes of observed RR spectra are pursued. The most recent results from RR studies of reaction intermediates of cytochrome *c* oxidase with the Fe^{II}–O–O–H and Fe^{IV}=O hemes are explained in detail. Finally RR spectra of reaction intermediates of iron–chlorin containing enzymes as well as those of catalase and thiolate-ligated heme enzymes are reviewed.

LIST OF ABBREVIATIONS

CAT	catalase
CCO	cytochrome *c* oxidase
CCP	cytochrome *c* peroxidase
CPO	chloroperoxidase
*m*CB	*m*-chlorobenzoate
*m*CPBA	*m*-chloroperbenzoic acid
EPR	electron paramagnetic resonance
^{NA}Fe	Fe in natural abandance, 92% pure ^{56}Fe
HRP	horseradish peroxidase
L	non-particular axial ligand
M	non-particular metal
Mb	myoglobin
2-MeIm	2-methylimidazole
N-MeIm	*N*-methylimidazole (1-methylimidazole)
MPO	myeloperoxidase
OEP	octaethylporphyrin dianion
P-450	cytochrome P-450
PPIX	protoporphyrin IX dianion
PPIXDME	protoporphyrin IX dimethylester dianion
$P_{piv}PP$	meso-tetrakis(α,α,α,α-*o*-pivalamidophenyl)porphyrin dianion (picket-fence porphyrin dianion)
RR	resonance Raman
salen	*N*,*N*′-ethylenebis(salicylideneiminato)
TDCPP	meso-tetrakis-2,6-dichlorophenyl porphyrin dianion
TMP	tetramesitylporphyrin dianion

TMPyP	meso-tetrakis(4-*N*-methylpyridiniumyl)porphyrin dianion
TPFPP	tetraperfluorophenylporphyrin dianion
TPP	tetraphenylporphyrin dianion

1. INTRODUCTION

Electrons around metal ions of metalloporphyrins can be regarded as if they were water in a small pond, irrigated by surrounding lakes through underground waterways. Removal of water from the pond is always partially replenished by the lakes and vice versa. This character endows metalloporphyrins with special physicochemical properties. "Highly oxidized metalloporphyrins" cover all porphyrins whose oxidation states are higher than trivial, whether the oxidative equivalent is located mainly at the metal ion or on the porphyrin macrocycle. In the latter case, however, it is classified as a porphyrin π cation radical and further grouped into the a_{1u} or a_{2u} type depending on the orbital of the unpaired electron. These two orbitals, which are conveniently represented under D_{4h} symmetry, are the nearly degenerate highest occupied porphyrin orbitals, but since their nodal patterns differ from each other, their physical properties exhibit dissimilarities.

In the case of iron porphyrin, the highly oxidized species include the ferryloxo (Fe^{IV}=O) neutral porphyrin, ferric and ferryloxo porphyrin π cation radicals, Fe^{V} neutral porphyrins, carbeniron porphyrins, and *N*-oxide porphyrins as illustrated in Fig. 1. The Fe^{IV} neutral porphyrin is commonly postulated as a catalytic intermediate of various heme enzymes including catalases, peroxidases, and oxidases, while active participation of the Fe^{IV}=O porphyrin π cation radical is proposed for catalytic reactions of some peroxidases, catalases, and cytochrome P-450. The *N*-oxide species might be involved in suicide reactions of cytochrome P-450. Certainly, the higher oxidation states of iron porphyrins are extremely important for catalytic reactions of heme enzymes, and, accordingly, understanding their properties in model compounds as well as enzymes themselves encompasses a basic subject of bioinorganic chemistry.

Resonance Raman (RR) spectroscopy has inspired the scientific field of porphyrin chemistry over the past two decades [1–4]. This is a technique that reveals only the vibrational spectra of a chromophore when its electronic absorption coincides with the wavelength of the Raman excitation light. Since the technique can be applied to heme proteins in aqueous solutions and metalloporphyrins in organic solutions, information on the electronic properties, including molecular structures, is obtainable. Thus, RR spectra have been extensively used to investigate various heme proteins and metalloporphyrins. Early studies during the 1970s uncovered structure–spectra correlations regarding ligation, oxidation, and spin states of the metal ion and core size of the porphyrins [5–11]. These empirical correlations serve as a guide in the interpretation of RR spectra observed for various heme proteins. One of the goals in RR studies of heme proteins is to elucidate the role of the protein surrounding

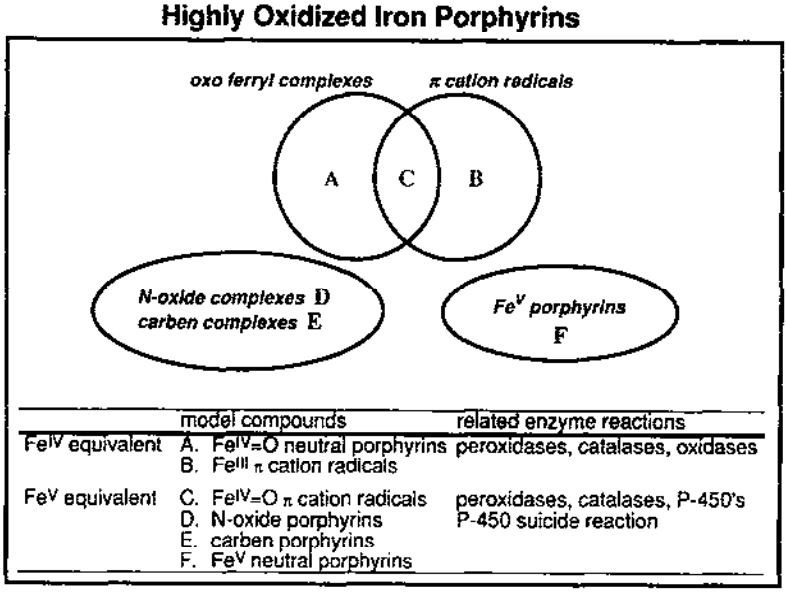

	model compounds	related enzyme reactions
Fe^{IV} equivalent	A. Fe^{IV}=O neutral porphyrins	peroxidases, catalases, oxidases
	B. Fe^{III} π cation radicals	
Fe^{V} equivalent	C. Fe^{IV}=O π cation radicals	peroxidases, catalases, P-450's
	D. N-oxide porphyrins	P-450 suicide reaction
	E. carben porphyrins	
	F. Fe^{V} neutral porphyrins	

Fig. 1. Categorization of highly oxidized iron porphyrins.

the heme by exploring how the properties and structures of iron porphyrins are altered on being captured into a heme pocket of proteins specific to each enzyme. For this purpose it is indispensable to observe RR spectra of reaction intermediates, i.e. highly oxidized heme proteins, and to correlate the RR data with the molecular structures, electronic structures, and especially reactivities of reaction intermediates. There are a few review articles along this line [12,13]. However, there has been no article that reviews the vicissitudes in interpretation of RR spectra of highly oxidized metalloporphyrins, despite the fact that controversies among different groups have been conspicuous. Accordingly, in this paper, we tried to provide a comprehensive survey of RR spectra of highly oxidized metalloporphyrins and heme proteins over the past decade (1983–1992) and to present the current situation with an emphasis on iron porphyrins. Attention will be paid to the metal–axial ligand bonds and their relation to the oxidation state of the metal and the macrocycles. For convenience, descriptions about metalloporphyrins and heme proteins are given separately in Sections 2 and 3 respectively.

2. RR SPECTRA OF HIGHLY OXIDIZED METALLOPORPHYRINS

2.1. Ferryloxo neutral porphyrins

2.1.1. Matrix isolation experiments

Efforts to detect the Fe^{IV}=O stretching RR band ($\nu(Fe^{IV}=O)$) of the ferryloxo porphyrins have been hampered by their thermal instability and photolability. The

pioneering work was carried out by Bajdor and Nakamoto [14] who succeeded in obtaining (TPP)Fe^{IV}=O (TPP, tetraphenylporphyrin dianion) by laser photolysis of the corresponding dioxygen adduct in O_2 matrix at 15 K, and their results are shown in Fig. 2, where full and broken lines denote the spectra for $(TPP)^{NA}Fe$ and $(TPP)^{54}Fe$ respectively, while spectra A, B, and C are for the complexes derived from $^{16}O_2$, $^{18}O_2$, and isotopically mixed dioxygen ($^{16}O_2$:$^{16}O^{18}O$:$^{18}O_2$ = 1:2:1) respectively. The 852 cm^{-1} band in spectrum A shifts to 818 cm^{-1} in spectrum B and two bands

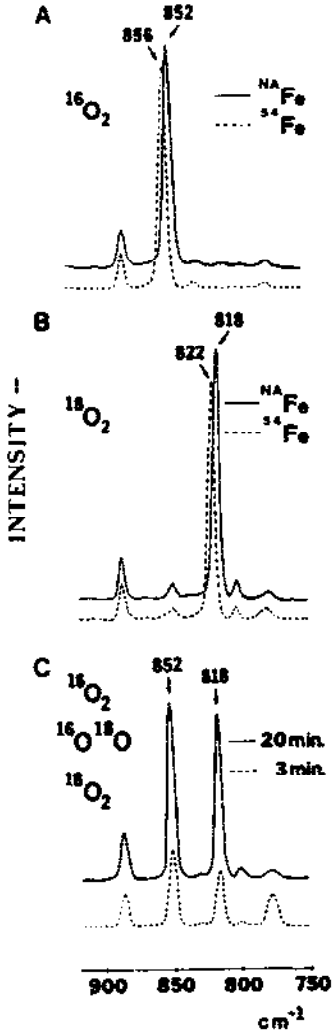

Fig. 2. RR spectra of (TPP)Fe on an O_2 matrix condensed at ≈15 K: spectra A, $(TPP)^{NA}Fe$ with $^{16}O_2$ (—) and $(TPP)^{54}Fe$ with $^{16}O_2$ (---); spectra B, $(TPP)^{NA}Fe$ with $^{18}O_2$ (—) and $(TPP)^{54}Fe$ with $^{18}O_2$ (---); spectra C, $(TPP)^{NA}Fe$ with isotopically mixed dioxygen ($^{16}O_2$:$^{16}O^{18}O$:$^{18}O_2$ = 1:2:1) recorded after 20 min (—) and 3 min (---) of laser irradiation. Laser, 406.7 nm. (Reproduced from ref. 14 with permission.)

appear at 852 and 818 cm^{-1} in spectrum C. The observed isotopic shift for $^{18}O_2$ (-34 cm^{-1}) is in good agreement with that expected for a diatomic Fe=O oscillator (-38 cm^{-1}). These bands cannot be assigned to the O–O stretching ($\nu(O^- - O^-)$) of (TPP)Fe–O–O–Fe(TPP), since these bands exhibited an upward frequency shift by 4 cm^{-1} on ^{54}Fe substitution as shown by broken lines, in good agreement with the $+3.5$ cm^{-1} shift expected for a diatomic Fe=O oscillator.

They extended similar experiments and observed the $\nu(Fe^{IV}=O)$ RR band at 852 cm^{-1} for (OEP)Fe^{IV}=O (OEP, octaethylporphyrin dianion) and at 851 cm^{-1} for (salen)Fe^{IV}=O (salen, *N,N'*-ethylenebis(salicylideneiminato)) [15]. The constancy of the $\nu(Fe^{IV}=O)$ frequencies indicates little coupling between the $\nu(Fe^{IV}=O)$ mode and internal vibrations of the macrocycle. For the low spin Fe^{IV} ion, the d_π(=d_{xz} and d_{yz}) and d_{xy} orbitals are occupied by one and two electrons respectively. Figure 3 illustrates the electron occupation in the Fe^{IV}=O unit and the $d(Fe^{IV})$–$p(O^{2-})$ interactions. The O^{2-} ligand with fully occupied p orbitals donates both σ and π electrons to the Fe^{IV} ion, filling their bonding molecular orbitals. The p orbitals of oxygen (p_x and p_y with z as the Fe–O direction) interact with d_π orbitals of Fe, but the antibonding contribution would increase as the increase in the d_π electrons. The p_z orbital of oxygen interacts with d_{z^2} orbital of metal, forming the σ bond. Occupation of electrons in the d_{z^2} orbital would increase the contributions of antibonding character. The d_{xy} and $d_{x^2-y^2}$ orbitals are in the porphyrin plane and, when the x axis is taken along the Fe–N (pyrrole) direction, d_{xy} and $d_{x^2-y^2}$ orbitals are non-

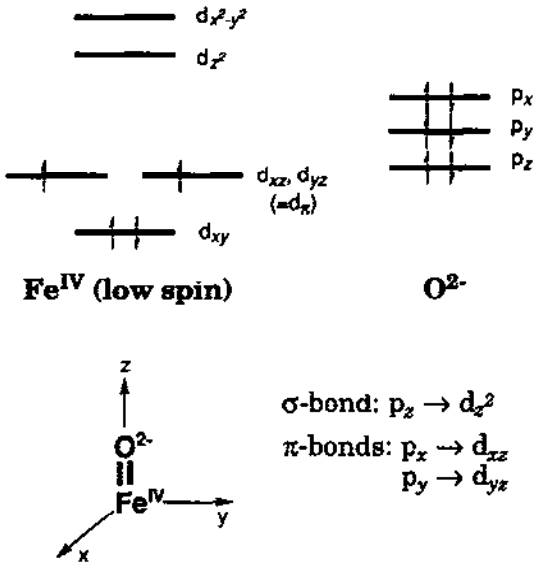

Fig. 3. Electron occupation in orbitals of the Fe^{IV}=O unit of the low spin ferryloxo porphyrin and the $p(O^{2-})$–$d(Fe^{IV})$ interactions (see text).

bonding and antibonding respectively with regard to the Fe–N (pyrrole) bonds. Therefore, $d_{x^2-y^2}$ is located much higher than other d orbitals.

This discussion suggests the bond order of the Fe^{IV}=O bond to be nearly 2. The force constant for the Fe^{IV}=O bond (estimated 5.32 mdyn $Å^{-1}$) is significantly larger than that for the Fe–O single bond (3.80 mdyn $Å^{-1}$ obtained from the μ-oxo dimer [(TPP)Fe^{III}–O–Fe^{III}(TPP)] [16]). Substantial π character is represented by $Fe^{IV}{\equiv}O^{2-}$ in which one σ bond (d_{z^2}–p_z overlap) and two π bonds (d_{xz}–p_x and d_{yz}–p_y overlaps) are involved.

2.1.2. Factors influencing the Fe^{IV}=O bond

Stimulated by the matrix experiments, several groups reported the ν(Fe^{IV}=O) RR bands of ferryloxo neutral porphyrins in solutions [17–27], and the ν(Fe^{IV}=O) frequencies and ^{18}O isotopic shifts so far reported are summarized in Table 1. As the factors which influence the Fe^{IV}=O bond strength, the following have been discussed: (i) trans ligation; (ii) porphyrin peripheral substituents; (iii) solvent; (iv) temperature. Since the ν(Fe^{IV}=O) frequency (820 cm^{-1}) of (PPIXDME)Fe^{IV}=O(*N*-MeIm) (PPIXDME, protoporphyrin IX dianion dimethylester; *N*-MeIm, *N*-methylimidazole) is not altered either by temperature change between −90 and −190°C or by porphyrin type (TPP vs. OEP) [19], factors (ii) and (iv) are considered to be less influential. This allows modification of the peripheral substituents of porphyrin and cryo measurements for studies of model compounds.

Spiro and co-workers thoroughly investigated factors (i) and (iii) for stable V^{IV}=O porphyrins, although the effect of radical formation on ν(V^{IV}=O) will be discussed later (see Section 2.3.1). They observed the ν(V^{IV}=O) RR bands of (OEP)V^{IV}=O, (TPP)V^{IV}=O, and (TMPyP)V^{IV}=O (TMPyP, mesotetrakis(4-*N*-methylpyridiniumyl porphyrin dianion)) in various solvents [28], and plotted the ν(V^{IV}=O) frequencies against the acceptor number of the solvent [29–31], which is a measure of its electrophilic character. The ν(V^{IV}=O) frequency decreases with an increase in the acceptor number. This means that the V^{IV}=O bond has a polar character and its O end interacts more strongly with solvent having the stronger acceptor character, retarding the O→V charge donation and thus resulting in weakening of the V^{IV}=O bond.

The ν(V^{IV}=O) frequencies were lower for the six-coordinate complexes than for the five coordinate. A vibrational coupling between the L–V and V=O stretching modes in a triatomic L–V=O oscillator gives a higher ν(V^{IV}=O) frequency than the diatomic V=O oscillator by 5–10 cm^{-1} when the diatomic ν(V^{IV}=O) frequency is located around 1000 cm^{-1} with a V–L stretching force constant of 1–2 mdyn $Å^{-1}$ and mass of L between 18 (water) and 65 (imidazole) [28]. The out-of-plane displacement of the V^{IV} ion from the mean porphyrin plane by 0.5 Å for the five-coordinate state [32] and no displacement for the six-coordinate state would also cause this difference. The amount of downshift in ν(V^{IV}=O) on ligation of the trans ligand increased with the increase of donor strength of the ligand. Therefore, it is likely

TABLE 1

Iron–oxygen stretching frequencies of ferryl oxo neutral porphyrins

Porphyrin complex	$\nu(Fe^{IV}=O)$ (cm^{-1})	$\Delta\nu(^{18}O)^a$ (cm^{-1})	Temperature (°C)	Solvent	References
$(TPFPP)Fe^{IV}=O$	854	−36	−250	Ar	[26]
$(TPP)Fe^{IV}=O$	852	−34	−250	Ar	[14]
$(OEP)Fe^{IV}=O$	852	−35	−258	Ar	[15]
$(salen)Fe^{IV}=O$	851	−35	−258	Ar	[15]
$(TPP)Fe^{IV}=O$	845	−33	−60	Toluene	[27]
$(OEP)Fe^{IV}=O$	845	−33	−60	Toluene	[27]
$(TMP)Fe^{IV}=O$	843	−36	−70	Toluene	[17,21]
$(TMP)Fe^{IV}=O$	845	−33	−46	Toluene	[24]
$(TMP)Fe^{IV}=O$	841	−36	−40	CH_2Cl_2	[23]
$(TDCPP)Fe^{IV}=O(THF)$	841	—	−50	THF	[20]
$(TDCPP)Fe^{IV}=O(DMF)$	829	—	−50	DMF	[20]
$(TDCPP)Fe^{IV}=O(N\text{-MeIm})$	818	—	−50	THF	[20]
$(PPIXDME)Fe^{IV}=O(N\text{-MeIm})$	820	−36	−120	Toluene	[19,22]
$(TPP)Fe^{IV}=O(N\text{-MeIm})$	820	−36	−120	Toluene	[19,22]
$(OEP)Fe^{IV}=O(N\text{-MeIm})$	820	−36	−120	Toluene	[19,22]
$(T_{piv}PP)Fe^{IV}=O(THF)$	829	−37	−50	THF	[18]
$(T_{piv}PP)Fe^{IV}=O(N\text{-MeIm})$	807	—	−50	THF	[18]
$(TMP_yP)Fe^{IV}=O$	818	—	RT	H_2O	[25]

[a] Isotopic frequency shift for ^{18}O substitution.

that the lower frequency for the six- than five-coordinate complexes is a reflection of strong electron donation from the trans ligand to the V^{IV} ion. Thus, the trans ligand effect can be understood on the same basis as for the solvent effect.

There has been no systematic study on the trans ligand effects for Fe^{IV}=O porphyrins owing to experimental difficulties. Figure 4 illustrates the $\nu(Fe^{IV}=O)$ RR band obtained by Kitagawa and co-workers [17,21] for (TMP)Fe^{IV}=O (TMP, tetramesitylporphyrin dianion). By using cryo RR spectroscopy, they pursued the following reactions which had been established by Balch et al. using nuclear magnetic

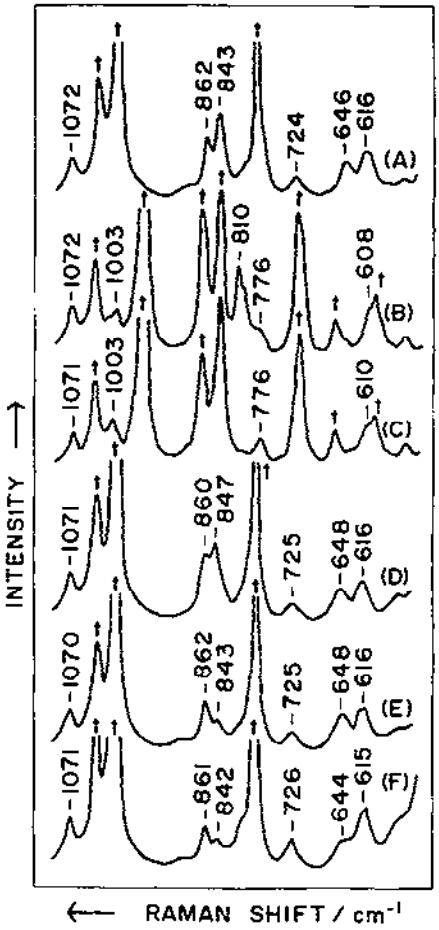

Fig. 4. Isotopic substitution effects of ferryloxo TMP on the RR spectra in the 1100–550 cm^{-1} region: spectrum A, $^{16}O_2$ derivative in toluene-h_8; spectrum B, $^{18}O_2$ derivative in toluene-d_8; spectrum C, $^{16}O_2$ derivative in toluene-d_8; spectrum D, ^{54}Fe and $^{16}O_2$ derivative in toluene-h_8; spectrum E, $^{16}O_2$ derivative after being warmed to −30°C and cooled to −70°C in toluene-h_8; spectrum F, (TMP)Fe^{III}–OH in toluene-h_8. †, Raman bands of solvent. (Reproduced from ref. 21 with permission.)

resonance (NMR) [33]:

$$(TMP)Fe^{II} + O_2 \rightarrow (TMP)Fe^{II}{-}O_2 \quad (1)$$

$$2(TMP)Fe^{II}{-}O_2 \rightarrow (TMP)Fe^{III}{-}O{-}O{-}Fe^{III}(TMP) + O_2 \quad (2)$$

$$(TMP)Fe^{III}{-}O{-}O{-}Fe^{III}(TMP) \rightarrow 2(TMP)Fe^{IV}{=}O \quad (3)$$

$$(TMP)Fe^{IV}{=}O + H \rightarrow (TMP)Fe^{III}{-}OH \quad (4)$$

The Fe^{II}–O_2 and O–O stretching RR bands of $(TMP)Fe^{II}$–O_2 in toluene at −100°C were identified at 522 cm^{-1} and 1171 cm^{-1} respectively. When the temperature was raised to −70°C, spectra A and B in Fig. 4 were observed for the $^{16}O_2$ derivative in toluene-h_8 and the $^{18}O_2$ derivative in toluene-d_8, respectively. A new band appeared at 810 cm^{-1} in spectrum B. When $^{16}O_2$ was used in toluene-d_8, the 810 cm^{-1} band disappeared and the band at 843 cm^{-1} was relatively intensified as shown by spectrum C, indicating that a solute band was overlapping with a solvent band at 841 cm^{-1}. Accordingly, the 843 cm^{-1} and 810 cm^{-1} bands should be associated with vibrations including motions of ^{16}O and ^{18}O respectively. If the species observed were the μ-peroxo dimer generated by reaction (2), the oxygen-isotope-sensitive band would be the O–O stretching ($\nu(O^- - O^-)$) mode of the peroxo bridge, and if the species observed were the ferryloxo complex generated by reaction (3), the band would be $\nu(Fe^{IV}{=}O)$. To distinguish those possibilities, the same experiment as that of spectrum A was carried out for the ^{54}Fe derivative, and the results are shown in spectrum D. Comparison of spectrum D with spectrum A indicates a 4 cm^{-1} upshift of the 843 cm^{-1} band with ^{54}Fe. The magnitudes of the observed frequency shifts (33 cm^{-1} for ^{16}O and ^{18}O and 4 cm^{-1} for ^{NA}Fe and ^{54}Fe) are closer to those expected for an Fe–O diatomic oscillator ($\Delta\nu = 37\ cm^{-1}$ for ^{16}O and ^{18}O and 3.4 cm^{-1} for ^{NA}Fe and ^{54}Fe) than that for an O–O diatomic oscillator ($\Delta\nu = 48\ cm^{-1}$ for ^{16}O and ^{18}O). Consequently, the 843 cm^{-1} band was assigned to $\nu(Fe^{IV}{=}O)$ and the species observed at −70°C was deduced to be $(TMP)Fe^{IV}{=}O$ contrary to the NMR study [33]. It is most likely that the μ-peroxo complex detected by NMR is extremely photolabile and immediately photoconverted to the ferryloxo complex on laser illumination. However, there is a report [27] that the Fe–O stretching RR band was observed at 573 cm^{-1} for $(TPP)Fe^{III}{-}O{-}O{-}Fe^{III}(TPP)$ in toluene at −80°C, where the coexisting 845 cm^{-1} band at −80°C was assigned to $\nu(Fe^{IV}{=}O)$ rather than to $\nu(O^- - O^-)$.

When the temperature of the sample used for the measurement of spectrum A in Fig. 4 was raised to −30°C and cooled to −70°C again, spectrum E was obtained. Spectrum E is practically the same as the spectrum of authentic $(TMP)Fe^{III}$–OH displayed as spectrum F. Thus the iron atom in $(TMP)Fe^{IV}{=}O$ is reduced to $(TMP)Fe^{III}$–OH at −30°C, in accordance with reaction (4). The spectral change from A to E in Fig. 4 was pursued in detail as a function of the period kept at −30°C and the results are illustrated in Fig. 5. Also plotted is the intensity of the

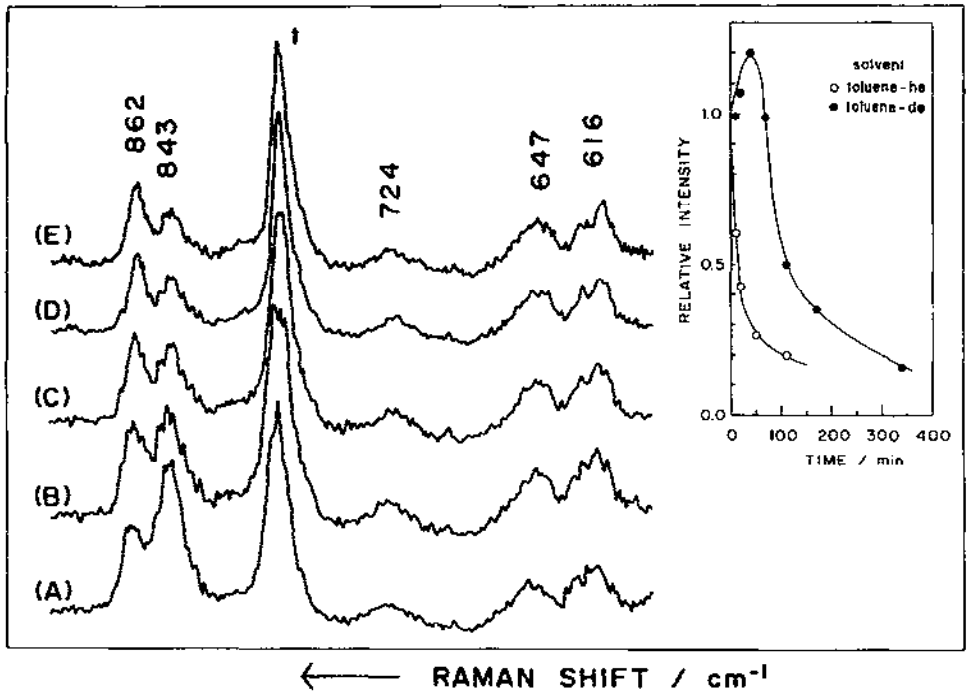

Fig. 5. Intensity change of the $\nu(Fe^{IV}=O)$ RR band due to the thermal decomposition of ferryloxo TMP. Spectrum A was observed in toluene-h_8 at −70°C just after preparation at −100°C, whereas spectra B–E were observed at −100°C after the sample was kept at −30°C for 10 min, 20 min, 50 min, and 110 min respectively. Also shown is the relative intensity of the $\nu(Fe^{IV}=O)$ RR band with respect to the solvent band (at 783 cm^{-1} for toluene-h_8 and at 869 cm^{-1} for toluene-d_8) plotted against the period in which the sample was kept at −30°C. †, solvent band used as reference. (Reproduced from ref. 21 with permission.)

$\nu(Fe^{IV}=O)$ RR band relative to that of the solvent band (at 783 cm^{-1} for toluene-h_8 and at 869 cm^{-1} for toluene-d_8). The decay of the $\nu(Fe^{IV}=O)$ RR band is found to be much faster in toluene-h_8 than in toluene-d_8. These observations suggest a kinetic isotope effect in the hydrogen transfer reaction between the ferryloxo complex and toluene to produce the ferric hydroxy complex. The solvent isotope effect is consistent with the studies by Gold et al. [20] who reported that the ferryloxo porphyrin π cation radical is more stable in CD_2Cl_2 than in CH_2Cl_2. The ferryloxo oxygen atom, which presumably has appreciable radical character, promotes hydrogen abstraction.

The RR spectrum observed at −70°C with a higher laser power (not shown) was coincident with the final spectrum obtained at −30°C with a low laser power, indicating that reduction of the ferryloxo to ferric hydroxy complex is promoted by laser illumination. This is probably due to enhancement of the radical character of the $Fe^{IV}=O$ bond on electronic excitation. Such intermixing of charge transfer character into the $\pi\pi^*$ state of the porphyrin ring might be the origin of the large relative intensity of the $\nu(Fe^{IV}=O)$ RR band on excitation within the Soret band.

Consequently, it is essential to use a low laser power for the measurement of RR spectra of the ferryloxo species.

The $\nu(Fe^{IV}=O)$ frequencies in Table 1 indicate that the influence of the trans ligand is large. In the absence of the trans ligand, $\nu(Fe^{IV}=O)$ is around 841–845 cm^{-1} in toluene, dichloromethane, and tetrahydrofuran (THF) solutions but, in the presence of a strong trans ligand such as *N*-MeIm, it shifts to 818–820 cm^{-1} for all porphyrin complexes studied. Since the trans ligand is both a strong σ donor and a moderate π donor, competitive electron donation to the Fe^{IV} ion tends to reduce donation from the oxo ligand and thus weakens the $Fe^{IV}=O$ bond. In this regard, the trans ligand influence on $\nu(Fe^{IV}=O)$ is qualitatively similar with that on $\nu(V^{IV}=O)$ but observed to be smaller in magnitude.

Solvent effects on $\nu(Fe^{IV}=O)$ frequencies appear qualitatively similar to those for vanadium–oxo complexes but have not been investigated systematically. The low $\nu(Fe^{IV}=O)$ frequency of the ferryloxo picket-fence porphyrin, $(T_{piv}PP)Fe^{IV}=O(THF)$, in THF (829 cm^{-1}) was interpreted in terms of the polarity of the pivalamide groups surrounding the oxo ligand, which would tend to reduce electron donation from oxygen to iron [22,28].

2.1.3. Other metal–oxo stretching modes

Comparison of $Fe^{IV}=O$ complexes with other metal–oxo (M=O) porphyrins would help our understanding of the nature of metal–oxo bonding. The ν(M=O) frequencies so far reported are summarized in Table 2, where the stretching force constants *K* are also listed to give an idea of the bond strength. On the increase of the atomic number of metal species in the fourth period, there is a slight increase in $\nu(M^{IV}=O)$ frequencies from V^{IV} to Cr^{IV}, a great decrease to Mn^{IV}, and a substantial increase to Fe^{IV}. Czernuszewicz et al. [35] explained this peculiar pattern in terms of the number of d electrons and special properties of the half-filled t_{2g}^3 (representation based on O_h symmetry) subshell.

TABLE 2

Resonance Raman M=O stretching frequencies for metalloporphyrins in solutions

	M	ν(M=O) (cm^{-1})	K^a (mdyn $Å^{-1}$)	References
Penta-coordinate form	V^{IV}	1007	7.26	[28]
	Cr^{IV}	1025	7.58	[34]
	Mn^{IV}	754	4.15	[35]
	Fe^{IV}	843	5.21	[17,21]
	Ru^{IV}	820	5.47	[27]
Hexa-coordinate form	Ru^{VI}	811	5.54	[27]
	Os^{VI}	877	6.37	[36]

[a] Calculated with a diatomic oscillator for a penta-coordinate form and with a triatomic oscillator for a hexa-coordinate form.

A V^{IV} ion has one d electron, which can be accommodated by the d_{xy} orbital, leaving the O–M π interactions unimpeded. Since there are two π overlaps besides the σ overlap (see Fig. 3), the M^{IV}–O^{2-} interactions result in a triple bond. A Cr^{IV} ion has two d electrons. Since the separation between d_{xy} and d_π is sufficiently large, the second d electron would occupy the d_{xy} orbital to yield a diamagnetic state without significantly changing the $M^{IV}\equiv O$ triple bond [34]. Since the effective nuclear charge is larger for the Cr^{IV} than V^{IV} ion, the force constant is slightly larger for the Cr^{IV}=O than the V^{IV}=O bond. For Fe^{IV} ion, two extra electrons are added and they are forced to occupy the d_π orbitals, which are antibonding about the M^{IV}=O bond. Accordingly, its bond order becomes 2, and thus a 31% reduction in the Fe^{IV}=O force constant is reasonably interpreted.

If the same d orbital pattern held for Mn^{IV} with d^3, the Mn^{IV}=O bond strength should be between those of Cr^{IV}=O and Fe^{IV}=O. Contrary to the expectation, its force constant is smaller than that for the Fe^{IV}=O bond. This is due to a different configuration of d electrons. The electron paramagnetic resonance (EPR) spectrum demonstrated the presence of three unpaired electrons, suggesting stabilization of the high spin configuration presumably due to the exchange interactions between three half-filled t_{2g} (=d_{xz} and d_{yz}) orbitals. Although the exchange interactions may lower the energy of d_π close to that of d_{xy}, occupation of two electrons in d_{xz} and d_{yz} is practically the same as the case of Fe^{IV}, but the effective positive charge is smaller for Mn^{IV} than for Fe^{IV}. Therefore, the force constant of the Mn^{IV}=O bond is smaller than that of the Fe^{IV}=O bond.

Paeng and Nakamoto [27] prepared (OEP)Ru^{IV}=O by mixing (OEP)Ru^{II} and dioxygen at −80°C in toluene-d_8 and observed the $\nu(Ru^{IV}=O)$ RR band at 820 cm^{-1} (779 cm^{-1} for the ^{18}O analogue). Similar experiments with (TPP)Ru^{II} gave the $\nu(Ru^{IV}=O)$ RR band at 780 cm^{-1} for the ^{18}O analogue (the corresponding $\nu(Ru^{IV}=^{16}O)$ band was hidden by the porphyrin band at 826 cm^{-1}).

The number of papers discussing the M^V state is limited. The Mo^V=O stretching bands were identified at 958 and 905 cm^{-1} for (TPP)Mo^V=O(OCH_3) and (TPP)Mo^V=O(NCS) respectively [37]. A stable manganese (V)–oxo tetraamide macrocycle was synthesized and its Mn^V=O stretching band was found at 979 cm^{-1} [38]. This is notably higher than the $\nu(Mn^{IV}=O)$ frequency in Table 2, in agreement with removal of an electron from the Mn^{IV}–O antibonding orbital. Very recently Yamaguchi et al. [39] succeeded in preparing a new type of high valent iron–oxo complex, (TDCPP)Fe^V=O (TDCPP 5,10,15,20-tetrakis-2,6-dichlorophenylporphyrin dianion) at −90°C and characterized it with UV–visible absorption, EPR, and deuterium NMR spectroscopies. Titration of it with iodide ion demonstrated that it is two electron oxidized from the Fe^{III} state and its EPR spectrum (g=4.33, 3.69, and 1.99 at 4.2 K) and solution magnetic susceptibility ($\mu_{eff}=4.0\pm0.2\ \mu_B$) indicated the high spin Fe^V ion ($S=3/2$). Observation of its $\nu(Fe^V=O)$ RR band is desirable. As an oxo M^{VI} porphyrin complex, Sun and Stein [36] synthesized (OEP)$Os^{VI}(O)_2$ and observed the symmetric $\nu(Os^{VI}=O)$ and $2\nu(Os^{VI}=O)$ RR bands at 877 and

1755 cm^{-1} on excitation near 580 nm. Accordingly, the 580 nm band was assigned to the $\pi(Os{-}O){\rightarrow}\pi^*(Os{-}O)$ transition. Paeng and Nakamoto [27] reported the symmetric $\nu(Ru^{VI}{=}O)$ frequencies at 811 cm^{-1} and 808 cm^{-1} for $(TMP)Ru^{VI}(O)_2$ and $(TPP)Ru^{VI}(O)_2$ respectively.

2.2. Metalloporphyrin π cation radicals

2.2.1. Two types of porphyrin cation radicals

The theoretical studies on electronic states of metalloporphyrins developed by Gouterman and co-workers [40] have elucidated that the two highest occupied molecular orbitals (HOMOs) are of a_{1u} and a_{2u} symmetry, being nearly degenerate under D_{4h} symmetry. One-electron oxidation of the porphyrin ring means abstraction of an electron from either the a_{1u} or the a_{2u} orbital, which results in the $^2A_{1u}$ or the $^2A_{2u}$ ground state respectively. The contour maps of these two orbitals obtained from ab initio calculations [41] are illustrated in Fig. 6. The nodal patterns and the coefficients for the constituent atoms are quite dissimilar between the two. The charge density of an unpaired electron resides at α (C_α) and β (C_β) carbon atoms in the a_{1u} radical whereas it lies mainly at the pyrrole nitrogen and meso carbon (C_m) atoms in the a_{2u} radical.

The distinction between the two types of radicals arose historically from the different reactivities of the reaction intermediates of catalases (CAT) and peroxidases which are typified by horseradish peroxidase (HRP). Peroxidase catalyses oxidation of various organic substrates (AH_2) with H_2O_2 as the specific oxidant (reaction (5)), while catalases dissociate H_2O_2 into H_2O and O_2 (reaction (6)):

peroxidases $H_2O_2+AH_2{\rightarrow}2H_2O+A$ (A, substrate) (5)

catalases $2H_2O_2{\rightarrow}2H_2O+O_2$ (6)

The two kinds of enzymes have some similarities; the resting state with an Fe^{III}–heme is physiologically active and in the enzyme reaction the heme is oxidized first by H_2O_2. The primary greenish intermediate detected spectrophotometrically in this oxidation is called "compound I" and one-electron reduction of it yields the brown–red second intermediate, called "compound II". While the primary reactions of CAT and HRP are the same, the visible absorption spectra as well as reactivities of compound I are different. On the contrary, electrochemical oxidation of $(OEP)Co^{III}X$ yielded two kinds of absorption spectra depending on the axial ligand ($X=Br^-$ or ClO_4^-) and they were ascribed to the a_{1u} or a_{2u} type of porphyrin π cation radicals [42]. On the basis of the similarity of their visible absorption spectra, HRP compound I was assumed to contain the a_{2u} porphyrin π cation radical and CAT compound I had the a_{1u} porphyrin π cation radical; the differences in their reactivity were then attributed to differences in radical types [43]. Recent studies [44–49], however, do not support this conclusion as described below, suggesting

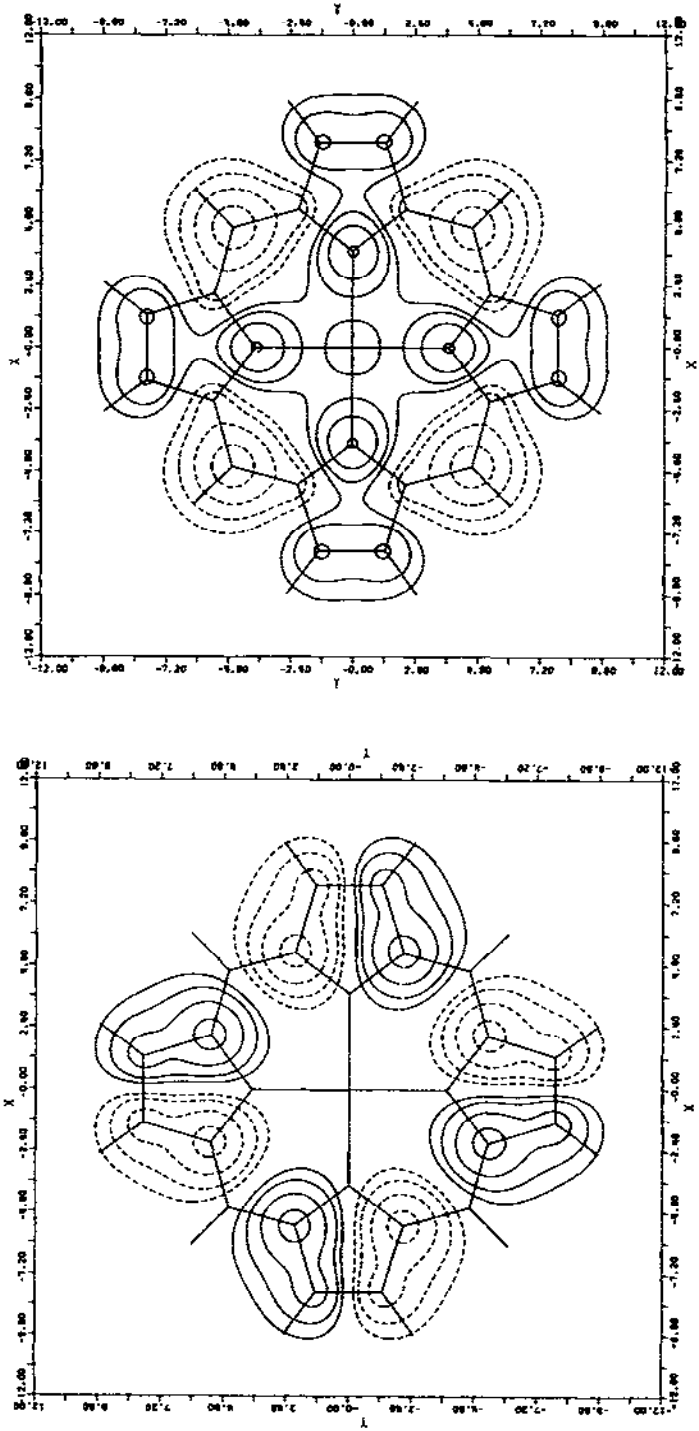

(a) (b)

Fig. 6. Contour maps of the highest occupied MOs with (a) a_{1u} and (b) a_{2u} symmetry in a plane 1.0 a.u. above the molecular plane. —, ---, contours of positive and negative values respectively. Their values are 0.01, 0.02, 0.04, 0.08, and 0.16. (Reproduced from ref. 41 with permission.)

that it is dangerous to use the optical spectra alone to diagnose the type of porphyrin π cation radicals.

2.2.2. RR Spectra of divalent metalloporphyrin radicals

In the RR spectra of porphyrin π cation radicals, the ν_2 mode which contains predominantly $C_\beta C_\beta$ and $C_\alpha C_m$ stretching and the ν_4 mode which mainly involves the $C_\alpha N$ and $C\alpha C_\beta$ stretching have attracted attention, because these two bands are expected to reflect differences in bond strength between the two kinds of porphyrin radicals and thus to be used as markers for distinguishing between them. Yamaguchi et al. [50] first reported the RR spectrum of metalloporphyrin π cation radicals, which were prepared through controlled potential electrolysis in CH_2Cl_2 for (TPP)M (M = Mg^{II}, Zn^{II}, and Cu^{II}), and their Raman shifts were consistent with the a_{2u} type. Subsequently the RR spectra of $(OEP^{+\cdot})M$ were reported by Kim et al. [51] and Salehi et al. [52] for several divalent metal species, although the spectra from these two groups were controversial.

Oertling et al. [53] discovered that the RR spectra of $(OEP^{+\cdot})M$ with a_{1u} character reported by Kim et al. [51] actually occurred from a demetallated impurity produced during the radical formation. In their subsequent paper [54] authentic RR spectra of $(OEP^{+\cdot})M(ClO_4)$ were obtained for M = Ni^{II}, Co^{II}, Cu^{II}, and Zn^{II}, and it was found that the frequencies of the modes mainly containing $C_\beta C_\beta$ stretching band were higher in the π cation radical than in the neutral species while those mainly associated with the $C_\alpha C_m$ and $C_\alpha N$ stretching were lower. Oertling et al. [54] demonstrated that the RR bands of $(OEP^{+\cdot})M$ in the 1450–1700 cm^{-1} region are metal dependent and are correlated with the porphyrin core size in the same way as with the neutral parent molecules, and accordingly inferred that the potential energy distributions in the normal modes of $(OEP^{+\cdot})M$ and (OEP)M are alike. They confirmed this conclusion by observing that the frequency shifts on deuteration of C_m and substitution of the C_β side chains are unaltered by the formation of a π cation radical [48]. Although in the early stage, Oertling et al. [48] thought that the RR frequencies in the 1450–1700 cm^{-1} region are insensitive to the a_{1u} or a_{2u} type on account of similarity in the RR spectra between $(OEP^{+\cdot})Co^{III}(ClO_4)$ and $(OEP^{+\cdot})Co^{III}Br$, they withdrew this idea [48], since the previously accepted assignments of $(OEP^{+\cdot})Co^{III}Br$ and $(OEP^{+\cdot})Co^{III}(ClO_4)$ to the a_{1u} and a_{2u} radicals respectively became suspicious [54]. The relationship between the radical type and the direction of the frequency shift from the frequency of the neutral species has been established through the extensive study by Czernuszewicz et al. [49]. Accordingly, the frequency shift patterns of the porphyrin modes on formation of a π cation radical are different between (OEP)M and (TPP)M; typical patterns for each are illustrated in Fig. 7 for the case of M = Cu^{II}. The ν_2 band shifts up for (OEP)M complexes but down for (TPP)M complexes. The shift directions of ν_2 are consistent with those expected from the nodal structures of the HOMO (Fig. 6) if the TPP and OEP radicals are of the a_{2u} and a_{1u} types respectively.

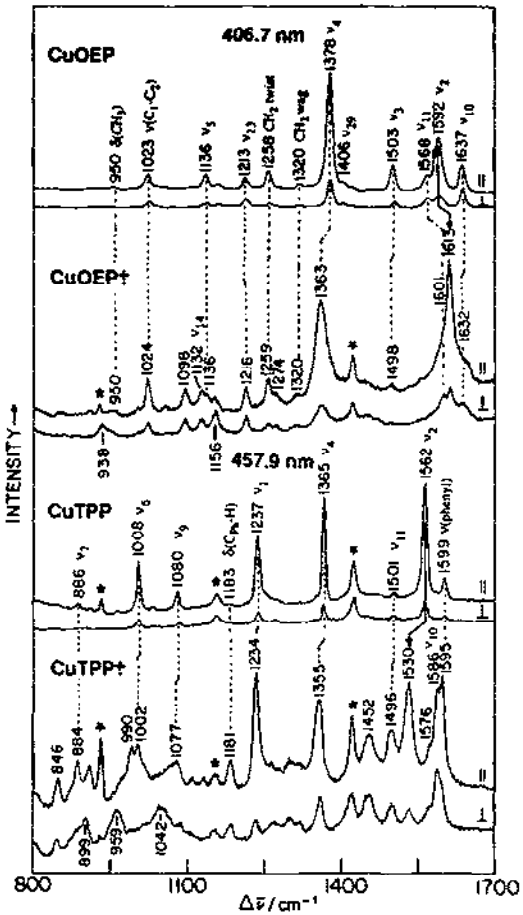

Fig. 7. Comparison of the RR spectra of (OEP)Cu^{II}–(OEP$^{+\cdot}$)Cu^{II} and (TPP)Cu^{II}–(TPP$^{+\cdot}$)Cu^{II}. Spectra were obtained with 406.7 nm ((OEP)Cu^{II} and (OEP$^{+\cdot}$)Cu^{II}) and 457.9 nm ((TPP)Cu^{II} and (TPP$^{+\cdot}$)Cu^{II}) excitation wavelengths, 50 mW laser power, and 8 cm^{-1} slit width. The ν_2 upshift for (OEP$^{+\cdot}$)Cu^{II} and downshift for (TPP$^{+\cdot}$)Cu^{II} are indicated with arrows. *, ClO_4^- (electrolyte) and CH_2Cl_2 solvent bands. (Reproduced from ref. 49 with permission.)

Czernuszewicz et al. [49] found that the 406.7 nm excited RR spectrum of (OEP$^{+\cdot}$)Ni^{II} exhibits prominent anomalously polarized Raman bands at 958 and 1166 cm^{-1} as shown in Fig. 8, where polarized RR spectra of (OEP$^{+\cdot}$)M are displayed for M = Zn^{II}, Ni^{II}, Cu^{II}, and V^{IV}=O. The frequencies of these two bands are sensitive to metal species and also to ^{15}N and meso deuterium substitutions. The isotope frequency shifts made it evident that these bands are not electronic Raman bands. Czernuszewicz et al. [49] considered that the A_{2g} vibrations of porphyrin π cation radicals are active to pseudo-Jahn–Teller (pJT) effects. When the ground state is $^2A_{1u}$, the first excited state should be $^2A_{2u}$ and vice versa. These two electronic states are nearly degenerate. The near degeneracy might possibly cause a pJT effect

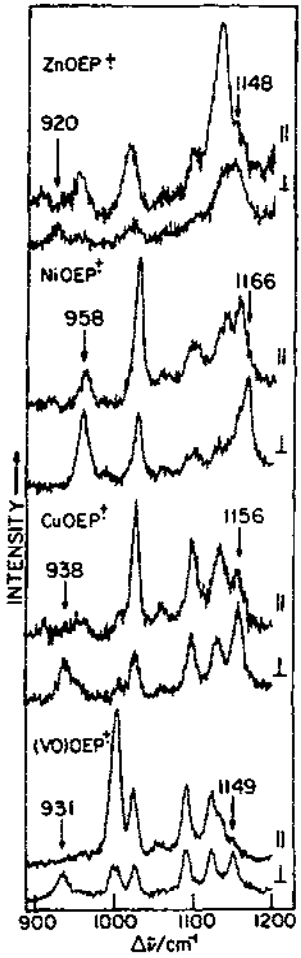

Fig. 8. Anomalously polarized bands in the Soret excited RR spectra of $(OEP^{+\cdot})Zn^{II}$, $(OEP^{+\cdot})Ni^{II}$, $(OEP^{+\cdot})Cu^{II}$ and $(OEP^{+\cdot})V^{IV}=O$. Spectra were obtained with 30–50 mW laser power and 8 cm^{-1} slit width using 406.7 nm (Ni, Cu, VO) and 363.8 nm (Zn) excitation wavelengths. (Reproduced from ref. 49 with permission.)

through a vibration whose symmetry is a cross product of the two electronic levels. $A_{1u} \times A_{2u} = A_{2g}$. Mixing of the two electronic levels is expected to result in more stabilization of the ground state, a larger energy separation between the ground and first excited state, and a shift to lower frequency of the mixing vibration. However, modes of the neutral porphyrin, corresponding to the RR bands at either 958 or 1166 cm^{-1}, could not be identified. Czernuszerwicz et al. [49] pointed out an interesting characteristic of π cation radicals, namely that the RR spectra excited by violet and yellow light, which are distinct in neutral metalloporphyrins, are similar to each other. This is, in fact, consistent with the observation by Oertling et al. [48].

2.2.3. RR spectra of iron porphyrin π cation radicals

2.2.3.1. In-plane vibrations The RR spectra of iron porphyrin π cation radicals were extensively investigated by Hashimoto et al. [55] and Oertling et al. [48,56]. The RR spectra of $(TMP^{+\cdot})Fe^{III}(ClO_4)_2$ and its isotopomers excited at 406.7 nm are shown in Fig. 9 [55], where polarized spectra for the unlabelled species are also displayed at the bottom. The RR spectrum was essentially unaltered by temperature

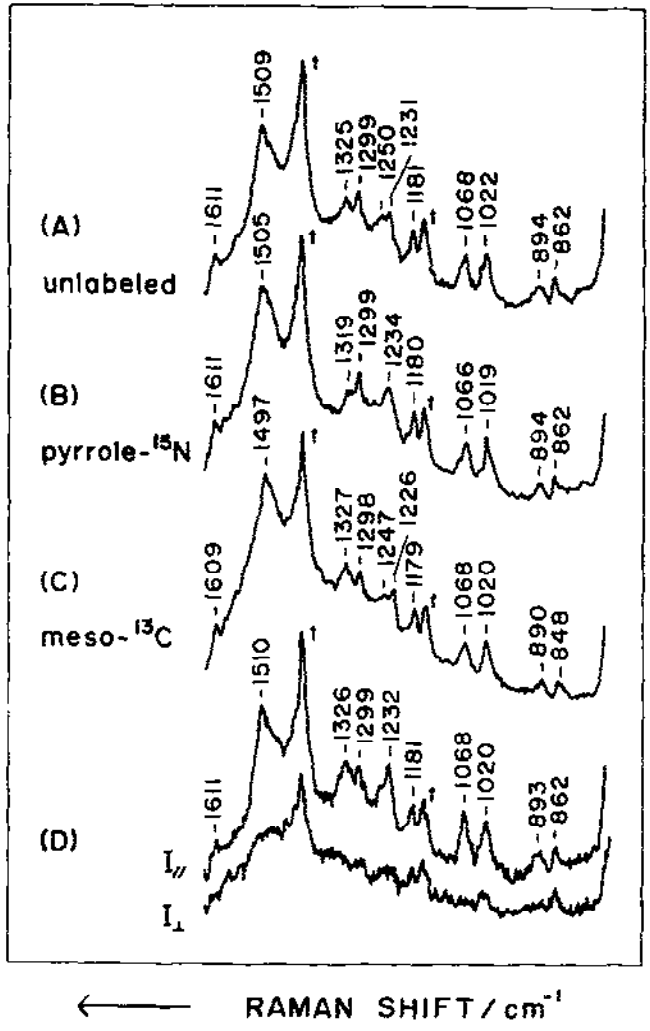

Fig. 9. RR spectra of $(TMP^{+\cdot})Fe^{III}(ClO_4)_2$ and its isotopomers in dried CH_2Cl_2 at room temperature: spectrum A, unlabelled species; spectrum B, pyrrole-^{15}N derivative; spectrum C, meso-^{13}C derivative; spectra D, polarized spectra for unlabelled species. †, due to solvent. The spectra were observed with a spinning cell. (Reproduced from ref. 55 with permission.)

changes between 10 and −100°C. The ferric porphyrin π cation radical is stable against laser illumination and accordingly the use of higher laser power did not yield any RR spectral changes. Although the absorbance of the Soret band is not particularly low [57], Raman bands of $(TMP^{+\cdot})Fe^{III}(ClO_4)_2$ are weak in comparison with the solvent (CH_2Cl_2) band at 1423 cm^{-1}. The polarized (p) RR band at 1325 cm^{-1} exhibits a frequency shift of −6 cm^{-1} on ^{15}N substitution and is therefore assigned to ν_4. Note that the ν_4 frequency of the π cation radical is distinctly lower than that of the ferric neutral porphyrins (1364–1368 cm^{-1}) [58], and its intensity reduction is noticeable. The depolarized (dp) band at 1250 cm^{-1}, which is probably buried under the 1234 cm^{-1} band for the ^{15}N derivative (B) but can be identified at 1247 cm^{-1} with the meso-^{13}C derivative (C), has a large $\Delta\nu(^{15}N)$ but a small $\Delta\nu(^{13}C)$, suggesting its assignment to be ν_{12} which mainly arises from the out-of-phase $C_\alpha N$ stretching mode. This is also downshifted from that of $(TMP)Fe^{III}Cl$ (1274 cm^{-1}). Although the vibrational mode of the π cation radical might be slightly altered from that of the neutral porphyrin, it is seen that the vibrations involving a $C_\alpha N$ stretching character are clearly shifted to lower frequencies in the π cation radical.

The assignment of an intense band at 1509 cm^{-1} (p), which exhibits a large downshift (−12 cm^{-1}) on meso ^{13}C substitution, is a key to the interpretation of this spectrum. In the Soret-excited RR spectra of divalent-metal porphyrin π cation radicals [48–54], the ν_2 band is most intense. Accordingly, it is likely that the 1507 cm^{-1} band of $(TMP^{+\cdot})Fe^{III}(ClO_4)_2$ arises from the ν_2 mode. On the contrary, the ν_2 mode of divalent-metal neutral porphyrins contains mainly the $C_\beta C_\beta$ and $C_\alpha C_\beta$ stretching but little $C_\alpha N$ stretching [58] and is expected to exhibit a moderate amount of ^{13}C shift but negligible ^{15}N shift. Actually, however, the 1507 cm^{-1} band of $(TMP^{+\cdot})Fe^{III}(ClO_4)_2$ exhibited an appreciable shift (−4 cm^{-1}) on ^{15}N substitution as well as on meso ^{13}C substitution (−12 cm^{-1}). It is therefore practical to say that the 1509 cm^{-1} band is assignable to ν_2. However, in this ν_2 mode the porphyrin π cation radical appreciably contains some $C_\alpha N$ stretching character and, consequently, is slightly different from the ν_2 modes of $(TPP)Ni^{II}$ and $(TMP)Fe^{III}Cl$ (see section 2.2.4).

The frequencies of other bands of $(TMP^{+\cdot})Fe^{III}(ClO_4)_2$ below 1240 cm^{-1} are not greatly different from those of $(TMP)Fe^{III}Cl$. Plausible assignments of Raman bands of $(TMP^{+\cdot})Fe^{III}(ClO_4)_2$ together with the polarization properties and isotopic frequency shifts are summarized in Table 3. Although the same mode numbers of neutral metalloporphyrin are used for the π cation radicals, actual vibrational modes would be appreciably different between the two species. These results indicate that removal of an electron from a porphyrin ring causes changes of a relatively limited number of double-bond stretching frequencies.

2.2.3.2. Phenyl modes The frequencies of the phenyl ring mode at 1611 cm^{-1} and C_m–C_{phenyl} stretching mode at 1231 cm^{-1} (Fig. 9, spectrum A) remain unaltered by ionization of the porphyrin ring in (TMP)Fe, suggesting that the electronic states of

TABLE 3

Observed frequencies, isotopic frequency shifts and the mode assignments for Raman bands of $(TMP^{+\cdot})Fe^{III}(ClO_4)_2$ (from ref. 55)

ν_i[a] (cm^{-1})	P[b]	$\Delta\nu(^{15}N)$[c] (cm^{-1})	$\Delta\nu(^{13}C)$[d] (cm^{-1})	Assignment
1611	p	0	−2	Phenyl (ν_{8a})
1509	p	−4	−12	ν_2
1325	p	−6	+2	ν_4
1299	p	0	−1	
1250	p	—	−3	ν_{12}
1231	p	+3	−5	ν_1
1181	dp	−1	−2	ν_{34}
1068	p	−2	0	ν_9
1022	dp	−3	−2	ν_{15}
894	p	0	−4	
862	dp	0	−14	ν_{32}

[a]Observed frequencies.
[b]Polarization (p, polarized; dp, depolarized).
[c]Isotopic frequency shift for ^{15}N substitution.
[d]Isotopic frequency shift for ^{13}C substitution.

phenyl rings are fairly well separated from those of the porphyrin ring. In contrast, for $(TPP)V^{IV}=O$ and $(TPP)Cu^{II}$, the phenyl mode becomes noticeably stronger on formation of the π cation radical [49], suggesting that the peripheral phenyl rings of TPP are more coplanar to the porphyrin plane to allow more delocalization of phenyl electrons to the half-filled radical orbital of porphyrin for $(TPP^{+\cdot})M$. As previously mentioned, the orbital density at C_m is large for the a_{2u} radical but zero for the a_{1u} radical. A minor change in the C_m–C_{phenyl} dihedral angle may alter the amount of π delocalization. If it takes place only in the excited state, the Soret excitation is accompanied by a conjugation change of the phenyl ring and we can expect intensity enhancement of the phenyl internal modes without a change in their ground state frequencies. In the case of $(TMP^{+\cdot})Fe$ π cation radicals, however, the internal rotation around the C_m–C_{phenyl} bond is hampered by the steric hindrance between two *o*-CH_3 groups of the phenyl substituents and the pyrrole groups of the porphyrin. Therefore, the π conjugation between the phenyl and porphyrin rings remains unchanged on electronic excitation even for the π cation radical. This would be a reasonable interpretation for RR intensity differences between the internal phenyl modes of $(TPP^{+\cdot})M$ and $(TMP^{+\cdot})Fe$.

If such torsion around the C_m–C_{phenyl} bond occurred in the ground electronic state of $(TPP^{+\cdot})M$ radicals, the radical property of the porphyrin ring might be slightly diluted owing to delocalization of electrons to the phenyl group. In fact, the leakage of the spin density to the phenyl ring has been detected in the EPR study

of $(TPP^{+\cdot})Zn^{II}$ [59–61]. Theoretical calculations on phenyl hyperconjugation [62], which would allow delocalization of π–σ spins into twisted phenyl rings, predicted larger leakage of the spin density for larger torsion around the C_m–C_{phenyl} bond. In a crystal, the phenyl group is nearly perpendicular to the porphyrin plane for (TMP)M [63] but is slightly rotated around the C_m–C_{phenyl} bond for (TPP)M [57]. If a similar torsion is present in the ground state of $(TPP^{+\cdot})M$ in solutions, this would influence the frequencies of double-bond stretching modes and cause some differences between RR spectra of $(TMP^{+\cdot})M$ and $(TPP^{+\cdot})M$ porphyrin π cation radicals.

2.2.4. Vibrational characters of π cation radicals

Detailed vibrational analysis has been worked out for neutral metalloporphyrins [58, 64, 65], although comparable studies have not been completed for the π cation radicals. Czernuszewicz et al. [49] stressed that negligible changes in the vibrational modes occurred between the neutral porphyrin and its π cation radical on the basis of their similar deuteration shifts. However, the ring-sensitive modes, ν_2 and ν_4, are actually not close to each other. Frequency changes on formation of the porphyrin π cation radical were $\Delta\nu_2 = -32\ cm^{-1}$ and $\Delta\nu_4 = -10\ cm^{-1}$ for $(TPP)Cu^{II}$ but were $\Delta\nu_2 = -53\ cm^{-1}$ and $\Delta\nu_4 = -43\ cm^{-1}$ for $(TMP)Fe^{III}(ClO_4)_2$. One plausible explanation for smaller shifts for $(TPP)Cu^{II}$ may involve differences between the radical character of the porphyrin ring in $(TPP^{+\cdot})Cu^{II}$ and $(TMP^{+\cdot})Fe^{III}(ClO_4)_2$ due to differences in π delocalization with the phenyl rings. In this regard, ^{13}C and ^{15}N isotopic frequency shifts for $(TPP^{+\cdot})Cu^{II}$ would be desirable but are at present not available. Since in π cation radicals an electron is removed from the π orbital which is bonding, non-bonding or antibonding with regard to a given bond, it is rather natural that the force constants and thus the potential energy distributions are appreciably altered from those of the neutral porphyrin. Currently the study on $(TMP^{+\cdot})Fe^{III}(ClO_4)_2$ is a sole report on the ^{13}C and ^{15}N isotopic frequency shifts of $(TPP^{+\cdot})M$-type π cation radicals.

Since the $C_\beta C_\beta$ bond is antibonding and bonding for the a_{1u} and a_{2u} HOMOs respectively [41], removal of an electron from the a_{1u} or a_{2u} orbital is expected to result in an upshift or a downshift of the $C_\beta C_\beta$ stretching vibration. The $C_\alpha N$ bond is non-bonding and antibonding for the a_{1u} and a_{2u} HOMOs [41]; a downshift is never expected for the $C_\alpha N$ stretching mode on formation of π cation radicals. Nonetheless, it is observed for $(TMP)Fe^{III}(ClO_4)_2$. This implies that significant configuration interaction should be incorporated after removal of electrons from the HOMOs illustrated in Fig. 6, and the resultant electronic state cannot be easily deduced from the ground state wavefunctions of neutral porphyrins.

2.2.5. Factors for determination of radical types

The original assignments of some $(OEP^{+\cdot})M$ radicals to a_{2u}, particularly for $M = Ni^{II}$, Cu^{II}, and Co^{III}–perchlorate adduct, and of $(OEP^{+\cdot})Co^{III}Br$ to a_{1u} were

based on the optical absorption spectra [66]. However, RR band frequency shifts due to the formation of π cation radicals did not distinguish between the two groups [54] and EPR [44] and NMR studies [45] also threw doubt on the assignments. On the basis of the magnitudes of the meso proton hyperfine constants, Sandusky et al. [47] demonstrated that the ground states of $(OEP^{+\cdot})Co^{III}Br$ and $(OEP^{+\cdot})Co^{III}(ClO_4)$ are predominantly $^2A_{1u}$ and the differences in their absorption spectra were ascribed to structural differences.

Czernuszerwicz et al. [49] demonstrated that all the $(OEP^{+\cdot})M$ and $(TPP^{+\cdot})M$ which they studied have a_{1u} and a_{2u} character respectively and offered a simple explanation based on the orbital pattern. Since the electron density at the C_m atoms is higher for the a_{2u} orbital but is zero for the a_{1u} orbital, the phenyl groups at C_m of TPP should raise the energy of the a_{2u} relative to the a_{1u} orbital via electronic repulsion between the filled phenyl and porphyrin π orbitals. In the case of OEP, the ethyl groups with an electron donating property would donate electrons to C_β. Both orbitals have appreciable density at C_β but the coefficients are slightly larger with the a_{1u} than a_{2u} orbitals and, accordingly, the a_{1u} level is raised more than the a_{2u} level. When the a_{1u} level is higher than a_{2u}, it would yield an a_{1u} π cation radical, in agreement with the observations. If this idea is correct, the relative energy between the a_{1u} and a_{2u} orbitals depends on the number of phenyl groups and also on the electron withdrawing ability of the phenyl substituents at C_m. Morishima and co-workers [67] introduced varied numbers of various phenyl groups to the meso position of (OEP)M and measured the NMR chemical shifts of the remaining meso protons for the π cation radicals. The ^1H signal shifted to lower field as the number of the meso-phenyl groups increased. The results were interpreted as due to the increasingly higher energy of the a_{2u} orbital relative to that of a_{1u} for the larger number of phenyl groups incorporated. Fujii and Ichikawa synthesized novel porphyrins which have chlorophenyl groups at C_β. The NMR spectra of these compounds suggested predominance of the a_{1u} character [68].

However, these arguments are applicable to metalloporhyrins with no or weak axial ligands. Extended Hückel calculations predicted that the a_{2u} orbital is increasingly destabilized relative to the a_{1u} orbital with stronger donor ability of the axial ligands [69]. Figure 10 illustrates a schematic energy diagram of the porphyrin and iron orbitals and possible effects of symmetry reduction from D_{4h} to C_{4v} on the low spin Fe^{IV}–porphyrin–axial ligands interactions. Here the HOMO of a porphyrin is assumed to be a_{2u}, and a lone pair in the p_z orbital of an axial ligand (L_{p_z}) is postulated to delocalize into the d_{z^2}(Fe) orbital to yield a σ-type bonding interaction ($d_{z^2}+L_{p_z}$). Accordingly, the presence of another electron in the d_{z^2}(Fe) orbital results in its occupation of the antibonding orbital (d_{z^2}-L_{p_z}). The oxo ligand donates σ and π electrons to the Fe^{IV} ion, while the imidazole (histidine) or phenolate (tyrosinate) ligand donates only σ electrons.

In D_{4h} symmetry there is no interaction between the HOMO of porphyrin (u symmetry) and any d orbitals (g symmetry), but their interaction is allowed under

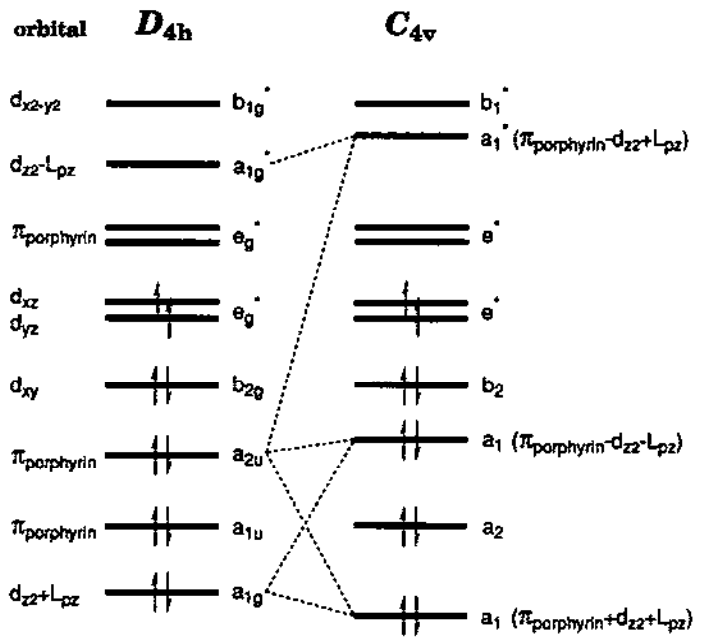

Fig. 10. Schematic energy diagram for the d orbitals of iron, the highest occupied a_{1u} and a_{2u} orbitals of porphyrin ring, and a lone pair orbital of an axial ligand (L_{p_z}), and effects of symmetry reduction from D_{4h} to C_{4v}. $d_{z^2}+L_{p_z}$ and $d_{z^2}-L_{p_z}$ represent the bonding and antibonding combination of the d_{z^2}(Fe) and p_z (axial ligand) orbitals. (Modified from ref. 70. See text.)

C_{4v} symmetry since both the a_{2u} (porphyrin) and d_{z^2}(Fe) orbitals belong to the a_1 species of C_{4v} (Fig. 10(b)). Such interaction does not occur for the a_{1u} porphyrin orbital. Since the electron density at the pyrrole nitrogen atoms is high for the a_{2u} orbital (zero for the a_{1u} orbital), the positive charge of a metal ion may stabilize the a_{2u} orbital and conversely, strong electron donation from the axial ligand counteracts it. Therefore, strongly donating axial ligands increasingly destabilize the a_{2u} orbital.

Since the symmetry character of the empty $4p_z$ (or $5p_z$) orbital of the metal ion is also a_{2u} under D_{4h} symmetry, the a_{2u} orbital of porphyrin is allowed to interact with the metal np_z orbital when the symmetry is lowered to C_{4v}. Usually this interaction is small because of a large separation of the two energy levels. However, when their energy separation happens to be small, the a_{2u} (porphyrin) level is strongly influenced by the interaction and the order of the a_{1u} (porphyrin) and a_{2u} (porphyrin) orbitals is reversed. In fact, Morishima and co-workers [71] demonstrated from NMR that both $(TMP^{+\cdot})Ru^{VI}(O)_2$ and $(OEP^{+\cdot})Ru^{VI}(O)_2$ adopt the $^2A_{1u}$ ground state. In this case the energy level of $5p_z$(Ru) orbital might be much lower than usual owing to its extremely high oxidation state.

When the size of the metal ion becomes larger than the core size of the porphyrin, the metal ion must go out of the porphyrin plane. This also lowers symmetry from D_{4h} to C_{4v}. The size effect of metal ions, which may raise the a_{2u}

level and thus result in the $^2A_{2u}$ ground state of porphyrin π cation radical, is seen in $(OEP^{+\cdot})OsCO$, for which Sun and Stein [36] demonstrated its a_{2u} character. Consequently, the empirical rule that $(OEP^{+\cdot})M$ and $(TPP^{+\cdot})M$ have the $^2A_{1u}$ and $^2A_{2u}$ ground states respectively is broken by $(TMP^{+\cdot})Ru(O)_2$ and $(OEP^{+\cdot})OsCO$ on account of the particular influence on the a_{2u} orbital as explained above.

2.3. *Ferryloxo porphyrin π cation radicals*

Recent studies have shown that the RR spectra of metalloporphyrin π cation radicals are sensitive to the effects of axial ligands as well as the metal species [48,49,54,56]. In order to discuss the properties of compound I of HRP and CAT, it is highly desirable to observe the RR spectra of ferryloxo porphyrin π cation radicals. Groves et al. [72] first succeeded in the preparation of a ferryloxo porphyrin π cation radical from $(TMP)Fe^{III}Cl$ and *m*-chloroperbenzoic acid (*m*CPBA) and demonstrated that the ferryloxo π cation radical has catalytic activity as a monooxygenase in contrast to the neutral ferryloxo porphyrins.

2.3.1. *Fe^{IV}=O stretching modes*

Hashimoto et al. [73] observed the $\nu(Fe^{IV}=O)$ RR band of a ferryloxo porphyrin π cation radical for the first time (Fig. 11). Spectra A and C were recorded in a spinning cell for the species obtained from the reaction of ^{16}O- and ^{18}O-*m*CPBA respectively with $(TMP)^{NA}Fe^{III}Cl$. The band at 828 cm^{-1} in spectrum A appeared only on formation of the π cation radical and this band shifted to 792 cm^{-1} with ^{18}O as shown by spectrum C. When the π cation radical was derived from $(TMP)^{54}Fe^{III}Cl$ and ^{16}O-*m*CPBA, spectrum E was obtained, with a new band at 832 cm^{-1}. The -36 cm^{-1} shift on ^{18}O substitution and 4 cm^{-1} shift on ^{54}Fe substitution are in agreement with theoretical isotopic frequency shifts expected for an Fe=O oscillator. Consequently, the 828 cm^{-1} band of spectrum A was assigned to $\nu(Fe^{IV}=O)$. When spinning of the cell was stopped, the $\nu(Fe^{IV}=^{16}O)$ and $\nu(Fe^{IV}=^{18}O)$ RR bands disappeared as shown by spectra B and D respectively indicating that the Fe^{IV}=O porphyrin π cation radical is photolabile.

Kincaid et al. [74] claimed that spectrum A in Fig. 11 might arise from a photoproduct, and located the $\nu(Fe^{IV}=O)$ RR band of the porphyrin π cation radical at 801 cm^{-1}. The photolability of the 828 cm^{-1} species in Fig. 11, spectrum A, had been noticed from its disappearance when the spinning of the cell was stopped. In response to the claim by Kincaid et al., Hashimoto et al. [55] examined the laser power dependence of the 828 cm^{-1} band and confirmed that its intensity relative to that of the porphyrin bands remained unaltered for laser powers between 5 and 0.5 mW, indicative of the photostability of the 828 cm^{-1} species. The discrepancy in these observations can be linked with differences in sample preparations. Hashimoto et al. [73] used solvent containing MeOH in accordance to a report by Groves et al. [72] who had stressed the importance of methanol (MeOH) as a stabilizer of the

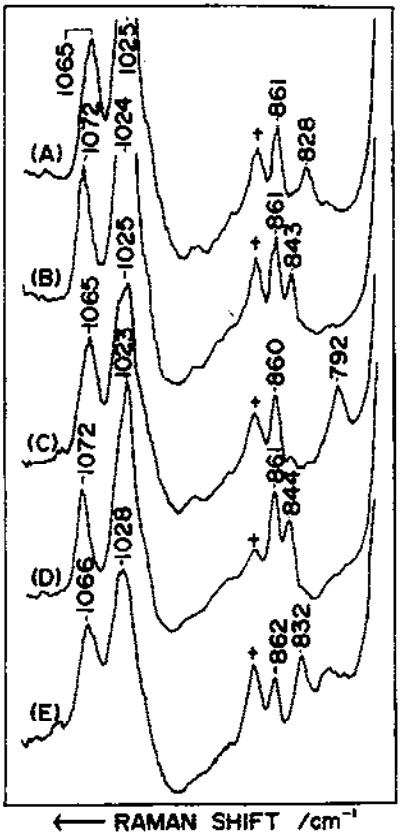

Fig. 11. RR spectra of $(TMP^{+\cdot})Fe^{IV}$=O observed at −80°C; spectrum A, the ^{16}O derivative with spinning cell; spectrum B, the ^{16}O derivative without spinning of the cell; spectrum C, the ^{18}O derivative with spinning cell; spectrum D, the ^{18}O derivative without spinning of the cell; spectrum E, the π cation radical derived from $(TMP)^{54}Fe^{III}Cl$ and ^{16}O-*m*CPBA. Excitation, 406.7 nm, 5 mW at the sample point. Accumulation time, 320 s. (Reproduced from ref. 72 with permission.)

Fe^{IV}=O porphyrin π cation radical, but Kincaid et al. [74] used an MeOH-free solvent to prepare the Fe^{IV}=O porphyrin π cation radical.

In order to solve this discrepancy Hashimoto et al. [55] examined the effects of MeOH on the RR spectra, and Fig. 12 shows the RR spectra of $(TMP^{+\cdot})Fe^{IV}$=O observed in the presence (full line) and absence (broken line) of MeOH. The difference in the α band is clear, although the difference in the Soret band was small. The band at 801 cm^{-1} in spectrum A is shifted to 804 cm^{-1} (spectrum B) when $(TMP)^{54}Fe^{III}Cl$ was used and to 764 cm^{-1} (spectrum C) when ^{18}O-labelled *m*CPBA was used. The upshift by 3 cm^{-1} and the downshift by 37 cm^{-1} on $^{56}Fe \rightarrow {}^{54}Fe$ and $^{16}O \rightarrow {}^{18}O$ replacement respectively agree with the expected shifts of $\Delta\nu(^{54}Fe) = +3.3$ and $\Delta\nu(^{18}O) = -35.2$ cm^{-1} calculated for a diatomic Fe=O harmonic oscillator. Therefore, this band was assigned to the $\nu(Fe^{IV}=O)$ bond of $(TMP^{+\cdot})Fe^{IV}$=O in the

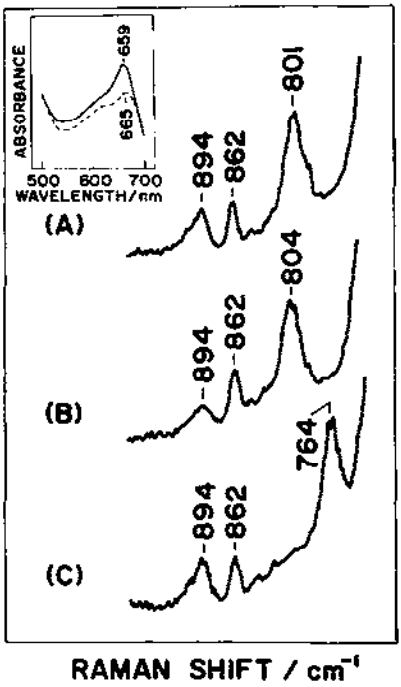

Fig. 12. RR spectra of $(TMP^{+\cdot})Fe^{IV}=O(mCB)$ in dried CH_2Cl_2 at −80°C: spectrum A, derived from ^{56}Fe porphyrin and ordinary *m*CPBA; spectrum B, derived from ^{54}Fe porphyrin and ordinary *m*CPBA; spectrum C, derived from ^{56}Fe-porphyrin and ^{18}O-*m*CPBA. Also shown are the absorption spectra in the α band region of $(TMP^{+\cdot})Fe^{IV}=O(MeOH)$ (—) and $(TMP^{+\cdot})Fe^{IV}=O(mCB)$ (---). (Reproduced from ref. 55 with permission.)

absence of MeOH, in agreement with Kincaid et al. [74]. When the laser power was raised, the 831 cm^{-1} band did not appear but the 801 cm^{-1} band simply disappeared. To gain further insight into the change of $\nu(Fe^{IV}=O)$ in the presence and absence of MeOH, various alcohols were added to the solvent and the RR spectra were measured as summarized in Fig. 13.

The $\nu(Fe^{IV}=O)$ RR band is seen at 831 cm^{-1} (spectrum A) and 801 cm^{-1} (spectrum E) in the presence and absence respectively of MeOH. However, these two bands are coexistent in the presence of ethanol (EtOH) (spectrum B; precisely 829 and 802 cm^{-1}) and 1-propanol (*n*-PrOH) (spectrum C, 829 and 801 cm^{-1}), while the frequencies of the other bands are scarcely altered. For the solution containing 2-methyl-2-propanol (*t*-BuOH), the 831 cm^{-1} band is missing (spectrum D) but the 801 cm^{-1} band is intense similar to spectrum E. In separate studies for $(OEP)Fe^{III}$(2-MeIm) [75, 76], coordination of MeOH, EtOH, and *n*-PrOH to Fe^{III} ion at the trans position of 2-MeIm was confirmed by observations of the Fe^{III}–alcohol stretching RR band and a charge transfer (CT) absorption band around 570–590 nm, but *t*-BuOH did not give such evidence for coordination. Accordingly,

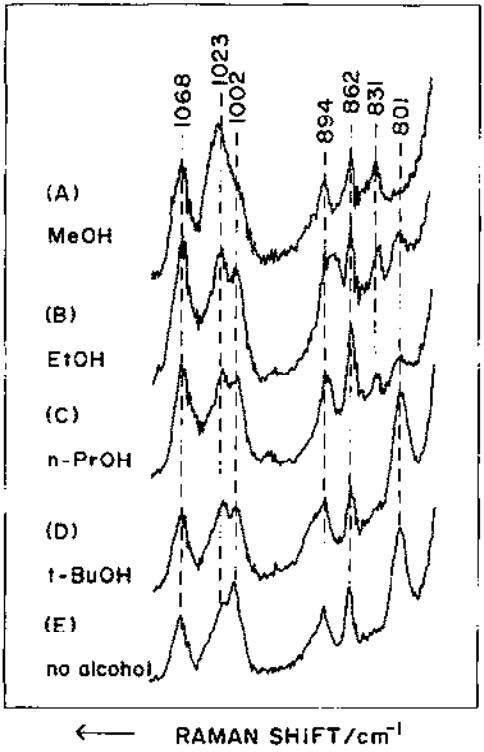

Fig. 13. RR spectra of $(TMP^{+\cdot})Fe^{IV}=O$(alcohol) and $(TMP^{+\cdot})Fe^{IV}=O$(*m*CB) at −80°C in dried CH_2Cl_2 with methanol (spectrum A), ethanol (spectrum B), *n*-propyl alcohol (spectrum C), or *t*-butyl alcohol (spectrum D), and in the absence of any alcohol (spectrum E). The spectra were observed with a spinning cell. (Reproduced from ref. 55 with permission.)

it is deduced that steric hindrance between the bulky alkyl group and pyrrole nitrogens obstructs coordination of *t*-BuOH. Consequently, the frequency difference in $\nu(Fe^{IV}=O)$ between Kincaid et al. [74] and Hashimoto et al. [73] was reasonably explained by the difference between alcohol-coordinated and non-coordinated compounds [55]. However, this was not compatible with the idea that the five-coordinate ferryloxo complexes generally give rise to higher $\nu(Fe^{IV}=O)$ frequencies than the six-coordinate complexes [14,15,18,19,21].

Previously, Groves and Watanabe [77] inferred that the product of *m*CPBA by its reaction with $(TMP)Fe^{III}Cl$, that is *m*-chlorobenzoate (*m*CB), was coordinated to the Fe^{IV} ion at the position trans to the oxo oxygen. In the presence of alcohol, *m*CB would compete with alcohol for coordination at the axial position, but the equilibrium is biased to alcohol owing to its higher concentration. In this case the frequency difference in $\nu(Fe^{IV}=O)$ should arise from the difference in σ donation of the trans ligand; the larger the σ donation, the lower the $\nu(Fe^{IV}=O)$ frequency. In fact, for ferryloxo neutral complexes, the $\nu(Fe^{IV}=O)$ frequency is lower when the

trans ligand is *N*-MeIm than when it is THF [18,20] (see Table 1). If the σ donation from *m*CB is larger than that of alcohol, the lower $\nu(Fe^{IV}=O)$ in the absence of alcohol is reasonably interpreted. One may argue that the ligand with higher σ donor property wins in the competition for coordination. It would be true if the concentration of *m*CB were the same as that of alcohol. Actually, however, the concentration of alcohol is much higher than that of *m*CB.

Su et al. [28] observed the upshifts of the $V^{IV}=O$ stretching ($\nu(V^{IV}=O)$) frequency of $(OEP)V^{IV}=O$ on formation of the π cation radical (a_{1u})) and ascribed it to the polarization effect of π electrons. They observed a 1.00% downshift of the $\nu(V^{IV}=O)$ band of $(OEP)^{IV}=O$ when the solvent was changed from benzene to CH_2Cl_2 and a 1.52% upshift on formation of a π cation radical in CH_2Cl_2 without a change in coordination number. On coordination of alcohol and a strong ligand such as imidazole to the V^{IV} ion at the position trans to oxygen, the $\nu(V^{IV}=O)$ frequency decreased by 2.35% and 5.99% respectively. If the same rate is applied to $(TMP)Fe^{IV}=O$ with $\nu(Fe^{IV}=O)$ at 843 cm^{-1} in toluene [21], the $\nu(Fe^{IV}=O)$ frequency of the five-coordinate neutral state in CH_2Cl_2 would be 835 cm^{-1} and a hypothetical five-coordinate $(TMP^{+\cdot})Fe^{IV}=O$ would have $\nu(Fe^{IV}=O)$ at 848 cm^{-1}. If *m*CB were regarded as a strong ligand like imidazolate, it would locate $\nu(Fe^{IV}=O)$ at 828 cm^{-1} for $(TMP^{+\cdot})Fe^{IV}=O$ (alcohol) and at 797 cm^{-1} for $(TMP^{+\cdot})Fe^{IV}=O$(*m*CB). These are in unexpectedly good agreement with the observed values. Therefore, the difference between the observed two $\nu(Fe^{IV}=O)$ frequencies is reasonably ascribed to the trans effect.

It is quite important to explore the radical type dependence of the $\nu(Fe^{IV}=O)$ frequency. Proniewicz et al. [26] measured RR spectra of the base-free dioxygen adducts of $(TPP)Fe^{II}$, $(OEP)Fe^{II}$, and $(TPFPP)Fe^{II}$ in the oxygen matrix at 30 K, and found two bands in the $Fe^{IV}=O$ stretching region; one at 861–853 cm^{-1} and the other at 815–809 cm^{-1}. The former and latter were assigned to the ferryloxo neutral and the a_{2u}-type ferryloxo porphyrin π cation radical respectively. This means a notable downshift of $\nu(Fe^{IV}=O)$ compared with the neutral species.

Macor et al. [70] studied the radical type dependence of the $V^{IV}=O$ stretching frequency for oxo–vanadium porphyrin π cation radicals. $(OEP)V^{IV}=O$ exhibited an upshift on formation of a π cation radical with the $^2A_{1u}$ ground state and attributed it to the increased O→V electron donation due to increased positive charge in the porphyrin ring. In contrast, the $\nu(V^{IV}=O)$ frequency was downshifted for $(TPP^{+\cdot})V^{IV}=O$ and $(TMP^{+\cdot})V^{IV}=O$ π cation radicals with the $^2A_{2u}$ ground state. The downshift was interpreted by mixing of the a_{2u}(porphyrin) orbital with d_{z^2} (vanadium) and p_z(oxygen) orbitals as discussed in section 2.2.5 (Fig. 10). This interaction, which is allowed under C_{4v} symmetry, results in partial delocalization of the V=O σ bonding electrons to the half-filled a_1(porphyrin) (a_{2u} in D_{4h} symmetry) orbital and thus in weakening of the V=O bond. Mixing of the a_2(porphyrin) (a_{1u} in D_{4h} symmetry) orbital with metal or oxygen orbitals is forbidden. However, it cannot be concluded that the downshift is inherent to $^2A_{2u}$ radicals, because in these

Fe^{IV}=O and V^{IV}=O complexes the metal ions are penta-coordinated and presumed to displace out of the porphyrin plane. From the biochemical point of view, it is highly desirable to examine a shift in the $\nu(Fe^{IV}=O)$ frequency on formation of the a_{2u} radicals in the hexa-coordinated form.

2.3.2. Porphyrin in-plane stretching modes

Hashimoto et al. [55] carried out vibrational assignments of the RR bands of a ferryloxo porphyrin π cation radical. Figure 14 shows the 406.7 nm excited RR spectra of $(TMP^{+\cdot})Fe^{IV}$=O and its isotopomers in CH_2Cl_2 containing MeOH. In contrast with $(TMP^{+\cdot})Fe^{III}(ClO_4)_2$, Raman bands of $(TMP^{+\cdot})Fe^{IV}$=O were generally found to be weak, probably because of the attenuated Soret absorbance, and the compound readily photodecomposed to $(TMP)Fe^{III}OH$ without spinning of the sample cell. Since the ν_4 band of $(TMP)Fe^{III}OH$ is not seen around 1364–1368 cm^{-1}, the sample for Fig. 14, spectrum A, seems not to contain the photodecomposed ferric compound. The spectrum did not change between −100 and −80°C but decomposed at higher temperatures. The 1358 cm^{-1} band of spectrum A was originally assigned

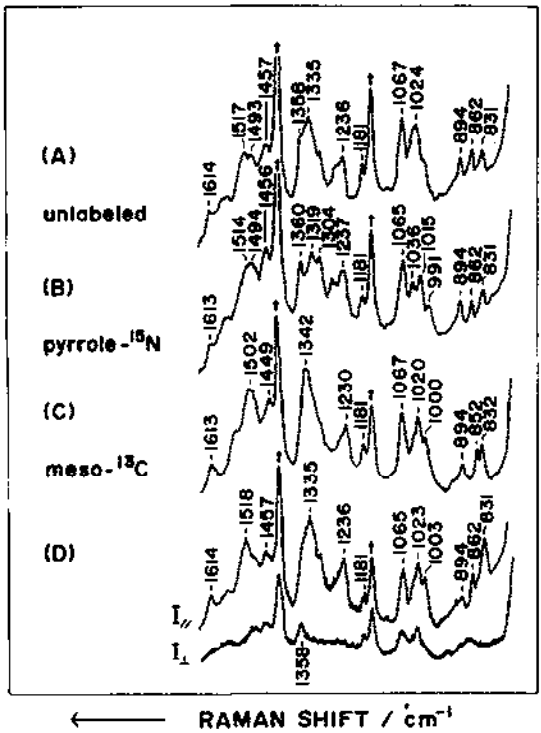

Fig. 14. RR spectra of $(TMP^{+\cdot})Fe^{IV}$=O(MeOH) and its isotopomers in CH_2Cl_2 containing MeOH at −80°C: spectrum A, unlabelled species; spectrum B, pyrrole-^{15}N derivative; spectrum C, meso-^{13}C derivative; spectra D, polarized spectra for unlabelled species. The spectra were observed with a spinning cell. †, due to solvent. The ratio of *m*CPBA to porphyrin was ca. 20. (Reproduced from ref. 55 with permission.)

to ν_4 by Kincaid et al. [74]. However, this band is depolarized and exhibits no frequency shift with ^{15}N substitution as shown by spectra D and B. On the contrary, the polarized band at 1335 cm^{-1} shifted to 1319 cm^{-1} on ^{15}N substitution and was therefore assigned to ν_4 by Hashimoto et al. [55]. This frequency is significantly lower than that of the ferryloxo neutral porphyrin; 1371 cm^{-1} for (TMP)Fe^{IV}=O [21].

The polarized band at 1517 cm^{-1} is shifted to 1514 cm^{-1} and 1502 cm^{-1} on ^{15}N and meso-^{13}C substitutions respectively and is assignable to ν_2. However, similar to the 1509 cm^{-1} band of (TMP$^{+\cdot}$)$Fe^{III}(ClO_4)_2$, it would not be the same mode as ν_2 of (TPP)Ni^{II} judging from the appreciable ^{15}N shift. The weak dp band at 1457 cm^{-1} might arise from ν_{11}, although it gives a large $\Delta\nu(^{13}C)$. Tentative assignments of other RR bands of (TMP$^{+\cdot}$)Fe^{IV}=O are summarized in Table 4 together with the observed frequencies [21] of the corresponding bands of the ferryloxo neutral porphyrin, (TMP)Fe^{IV}=O.

The common and characteristic features of (TMP$^{+\cdot}$)Fe^{IV}=O(MeOH) and (TMP$^{+\cdot}$)$Fe^{III}(ClO_4)_2$ are the considerable downshift of the ν_4 frequency. It is difficult to deduce how close the ν_4 mode of (TMP$^{+\cdot}$)Fe^{IV}=O(MeOH) is to that of (TPP)Ni^{II}, since the peak position of the ^{13}C isotopomer of the former is obscured in Fig. 14, spectrum C. The large value of $\Delta\nu(^{15}N)$ suggests a significant contribution from the $C_\alpha N$ stretching mode. Accordingly, the formation of a π cation radical with

TABLE 4

Observed frequencies, isotopic frequency shifts and the mode assignments for Raman bands of (TMP$^{+\cdot}$)Fe^{IV}=O(MeOH) and the corresponding data for (TMP)Fe^{IV}=O

(TMP$^{+\cdot}$)Fe^{IV}=O(MeOH)[a]					(TMP)Fe^{IV}=O[b]
ν_i (cm^{-1})	P	$\Delta\nu(^{15}N)$ (cm^{-1})	$\Delta\nu(^{13}C)$ (cm^{-1})	Assignment	ν_i (cm^{-1})
1614	p	−1	−1	Phenyl (ν_{8a})	—
1517	p	−3	−15	ν_2	1570
1457	dp	−1	−8	ν_{11}	—
1358	dp	+2	−16		—
1335	p	−16	−	ν_4	1371
1236	p	+1	−6	ν_1	1229
1181	dp	0	0	ν_{34} or ν_{17}	—
1067	p	−2	0	ν_9	1071
1024	dp	−9	−4	ν_{15}	—
1003	p	−12	-3	ν_6	—
894	p	0	0		—
862	dp	0	−10	ν_{32}	862
831	p	0	+1	$\nu(Fe^{IV}=O)$	843

[a] From ref. 55.

[b] From ref. 21.

(TMP)Fe^{III} and (TMP)Fe^{IV}=O is accompanied by weakening of the $C_\alpha N$ bonds and/or the vibrational mode itself becomes more pure $C_\alpha N$ stretching. This contrasts with the case of (TPP)V^{IV}=O which only exhibits a 2 cm^{-1} downshift in ν_4 on formation of the π cation radical [70].

RR spectra of (TMP$^{+\cdot}$)Fe^{IV}=O obtained in the absence of MeOH are displayed in Fig. 15 [55]. Frequencies of most bands and their behaviour on isotopic substitutions bear close resemblance between Figs. 14 and 15 except for a few points. In the absence of MeOH, a prominent RR band at 1355 cm^{-1} exhibits no shift on ^{15}N substitution but is shifted to a lower frequency by 6 cm^{-1} on ^{13}C substitution. The ν_4 band, which should be polarized and is expected to shift on ^{15}N substitution, cannot be identified in Fig. 15. This band might be buried in a wing of the 1355 cm^{-1} band, but the difference spectra, (TMP$^{+\cdot}$)Fe^{IV}=O minus (^{15}N-TMP$^{+\cdot}$)Fe^{IV}=O, failed to reveal the presence of a ^{15}N isotope-sensitive band. A new band appears at 1526 cm^{-1}, which exhibits frequency shifts of -4 cm^{-1} and -8 cm^{-1} on ^{15}N and ^{13}C substitution respectively, similar to the 1509 cm^{-1} band of (TMP$^{+\cdot}$)$Fe^{III}(ClO_4)_2$, and is considered to arise from the modified ν_2 mode. It is noted that the relative

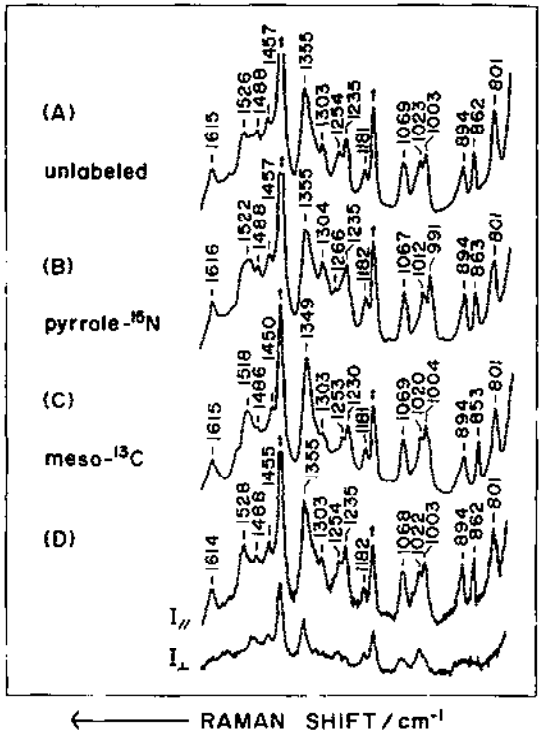

Fig. 15. RR spectra of (TMP$^{+\cdot}$)Fe^{IV}=O(*m*CB) and its isotopomers in dried CH_2Cl_2 at -80°C: spectrum A, unlabelled species; spectrum B, pyrrole-^{15}N derivative; spectrum C, meso-^{13}C derivative; spectra D, polarized spectra for unlabelled species. The spectra were observed with a spinning cell. †, due to solvent. The ratio of *m*CPBA to porphyrin was ca. 2. (Reproduced from ref. 55 with permission.)

intensity of the band at 1003 cm^{-1} is high and an intense band appears at 801 cm^{-1} in the spectra of $(TMP^{+\cdot})Fe^{IV}=O$ in comparison with those of $(TMP^{+\cdot})Fe^{IV}=O(MeOH)$.

The ferryloxo porphyrin π cation radical spectra presented in Figs. 14 and 15 are characterized by large downshifts of both ν_2 and ν_4, and therefore are categorized as a_{2u}-type radicals, which is in agreement with the NMR study [72]. Since the RR spectrum did not reveal any temperature dependence for both Fe^{III}– and $Fe^{IV}=O$ porphyrin π cation radicals, coexistence of two kinds of radicals [67] is unlikely. In other words, the energy separation between the a_{1u} and a_{2u} orbitals is fairly large. For a further step it is desirable to establish the RR spectra of a_{1u}-type ferryloxo π cation radicals and to examine radical type dependence of the ν_2 and ν_4 frequencies. Finally, it seems critical that Fujii [78] recently synthesized four a_{1u}- and four a_{2u}-type $Fe^{IV}=O$ porphyrin π cation radicals characterized by NMR and concluded that the monooxygenase activity of the ferryloxo oxygen does not depend on the radical types discussed above.

2.4. Other highly oxidized iron–porphyrin complexes

2.4.1. Nitridoiron porphyrins

The observation that liver microsomal cytochrome P-450 LM3,4 catalyses nitrogen atom transfer [79] suggests that a multiple $Fe^{V}\equiv N$ bond similar to the $Fe^{IV}=O$ bond is involved in the reaction cycle. Wagner and Nakamoto [80,81] investigated the RR spectra of nitridoiron porphyrin, which might be regarded as a model for intermediates of the nitrogen transfer reaction. The compound was produced by laser irradiation of thin films of the ferric azide adduct at 30 K and the $Fe^{V}\equiv N$ stretching ($\nu(Fe^{V}\equiv N)$) RR band was identified at 876 cm^{-1} for OEP and TPP complexes and at 873 cm^{-1} for a TMP complex. The ν_4 frequencies were close to those of the corresponding $Fe^{IV}=O$ compounds, eliminating the possibility of π cation radical.

The $\nu(M^{V}\equiv N)$ RR bands for other porphyrins include 1017 cm^{-1} for $Cr^{V}\equiv N$ [82] and 1049–1052 cm^{-1} for $Mn^{V}\equiv N$ [83–85]. Tsubaki et al. [86] observed the $\nu(M^{V}\equiv N)$ RR band of $(PPIX)Mn^{V}\equiv N$ incorporated into apoproteins of Mb and HRP at 1010 cm^{-1} and 1003 cm^{-1} respectively, which were substantially lower than that (1046 cm^{-1}) observed for 0.1 N aqueous NaOH solution of the complex. The porphyrin ring vibrations were also greatly influenced on incorporation into the apoproteins, suggesting core expansion of porphyrin in the protein possibly due to coordination of an amino acid residue to Mn^{V} trans to nitrogen [86].

2.4.2. N-oxide porphyrin

The ferryloxo porphyrin π cation radical is the most likely candidate for the ultimate oxidizing intermediate in the catalytic cycle of cytochrome P-450 [87,88]. However, an alternative active intermediate is an N-bridged iron–porphyrin *N*-oxide

suggested on the basis of the crystal structures of N-bridged iron–porphyrin carbenes [89–91] and the presence of other metalloporphyrin *N*-oxides [92–94]. Furthermore, MO calculations have predicted that Fe^{III}–porphyrin *N*-oxide is more stable than the isomeric Fe^{IV}=O porphyrin π cation radical [95–97].

Groves and Watanabe [98] first prepared and characterized the Fe^{III}–porphyrin *N*-oxide, which was found to be distinct from the isomeric Fe^{IV}=O porphyrin π cation radicals and to have no monooxygenase activity [99]. Mizutani et al. [100] observed the RR spectra of the *N*-oxide complex and its ^{15}N and ^{18}O analogues, which are shown in Fig. 16(A) (1200–700 cm^{-1}) and 16(B) (600–400 cm^{-1}). Spectra a and c in Fig. 16(B) show the RR spectra of the *N*-oxide complex derived from ^{16}O-*m*CPBA oxidation of $(TMP)^{NA}Fe^{III}$–OH and $(TMP)^{54}Fe^{III}$–OH respectively, while spectra b and d are their ^{18}O counterparts. The RR band at 506 cm^{-1} (spectrum a) is downshifted to 498 cm^{-1} (spectrum b) on ^{16}O–^{18}O substitution. When the ^{54}Fe-substituted porphyrin was used, the RR band at 506 cm^{-1} in spectrum a and at 498 cm^{-1} in spectrum b upshifted to 507 cm^{-1} in spectrum c and to 500 cm^{-1} in spectrum d respectively. Accordingly, the 506 cm^{-1} band is assigned to the Fe^{III}–O stretching mode (ν(Fe^{III}–O)). The ν(Fe^{III}–O) frequency

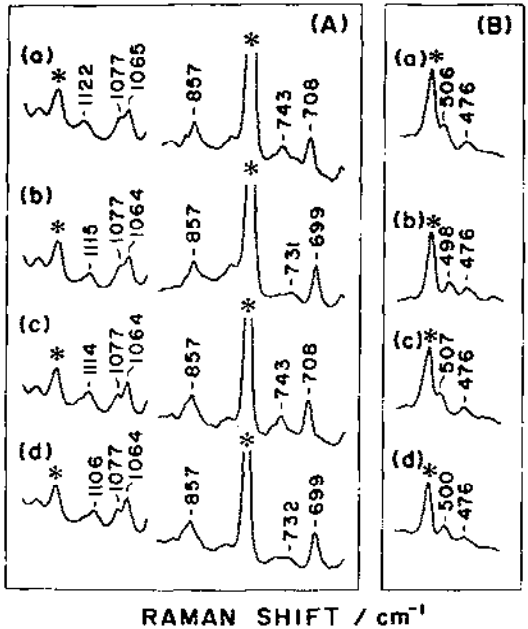

Fig. 16. RR spectra of *N*-oxide complex in (A) 1200–650 cm^{-1} and (B) 600–400 cm^{-1} regions. (A) Spectrum a, ^{16}O and ^{NA}N derivative; spectrum b, ^{18}O and ^{NA}N derivative; spectrum c, ^{16}O and ^{15}N derivative; spectrum d, ^{18}O and ^{15}N derivative. (B) Spectrum a, ^{16}O and ^{NA}Fe derivative; spectrum b, ^{18}O and ^{NA}Fe derivative; spectrum c, ^{16}O and ^{54}Fe derivative; spectrum d, ^{18}O and ^{54}Fe derivative. *, Raman bands of solvent. (Reproduced from ref. 100 with permission.)

is close to those of ferric hydroxy porphyrins (490–495 cm^{-1}) [101,102] and the ferric methoxy complex (524 cm^{-1}) [75,103].

Traces a and c in Fig. 16(A) show the RR spectra of the *N*-oxide complexes derived through ^{16}O-*m*CPBA oxidation of (^{NA}N-TMP)Fe^{III}–OH and (^{15}N-TMP)Fe^{III}–OH respectively, and traces b and d are their ^{18}O counterparts. In this frequency region, three oxygen-isotope-sensitive bands are seen at 1122, 743, and 708 cm^{-1}. The 1122 cm^{-1} band, which exhibits ^{14}N–^{15}N and ^{16}O–^{18}O isotopic frequency shifts, is assigned to the N–O stretching (ν(N–O)) mode. The 743 and 708 cm^{-1} bands are sensitive only to the mass of oxygen and are assignable to the Fe–O–N bending vibration, although the appearance of two bands remains to be explained. In this case, the presence of the Fe–O–N bridge in a solution of the *N*-oxide complex was established by the observation of ν(Fe^{III}–O) and ν(N–O) RR bands.

Figure 17 compares the RR spectra of (^{NA}N-TMP)Fe^{III}–OH (spectrum a) and (^{15}N-TMP)Fe^{III}–OH (spectrum b) with those of the corresponding products derived through ^{16}O-*m*CPBA oxidation (spectra c and d respectively). The ν_2 and ν_4 bands of (TMP)Fe^{III}OH are identified at 1554 cm^{-1} and 1361 cm^{-1} respectively. The corre-

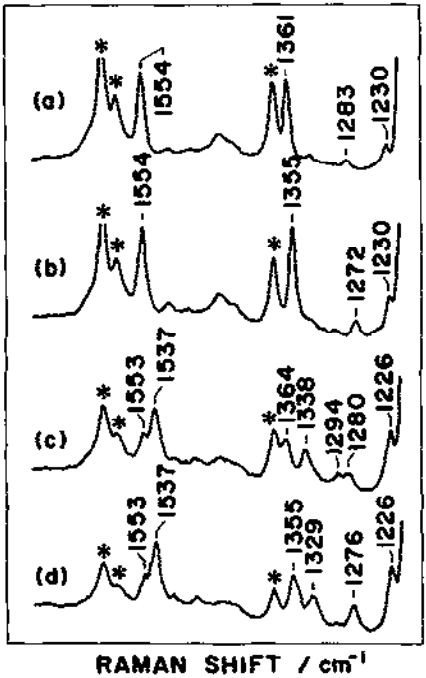

Fig. 17. RR spectra of (TMP)Fe^{III}–OH and *N*-oxide complexes in a high frequency region: spectrum a, unlabelled (TMP)Fe^{III}–OH; spectrum b, pyrrole-^{15}N labelled (TMP)Fe^{III}–OH; spectrum c, *N*-oxide species derived from unlabelled (TMP)Fe^{III}–OH; spectrum d, *N*-oxide species derived from pyrrole-^{15}N labelled (TMP)Fe^{III}–OH. *, Raman bands of solvent. (Reproduced from ref. 100 with permission.)

sponding bands of the *N*-oxide complex are observed at 1553 and 1537 cm^{-1} for ν_2 and at 1364 and 1338 cm^{-1} for ν_4. The higher frequency counterpart of the doublets, whose frequencies are close to those of the parent molecule, cannot be attributed to unreacted (TMP)Fe^{III}–OH because the visible absorption spectra indicated the concentration of (TMP)Fe^{III}–OH to be low enough and the excitation wavelength (441.6 nm) is more favourable for the *N*-oxide complex (λ_{max} = 440 nm) than to (TMP)Fe^{III}–OH (λ_{max} = 417 nm). This splitting presumably reflects coexistence of the bridged and non-bridged pyrrole rings. Similar splittings of ν_2 and ν_4 are reported for metallotetraphenylchlorin [104].

3. RR SPECTRA OF HIGHLY OXIDIZED HEME PROTEINS

3.1. Ferryloxo neutral porphyrin intermediates

The RR spectra of reaction intermediates of heme enzymes, which contain the ferryloxo neutral porphyrin, have been identified for five kinds of peroxidases so far, two kinds of terminal oxidases isolated from bovine heart and *Escherichia coli*, and a catalase of bovine liver. The observed $\nu(Fe^{IV}=O)$ frequencies are summarized in Table 5, and methods for observing time-resolved RR spectra of reaction intermediates of enzymes are described elsewhere [13].

TABLE 5

Iron–oxygen stretching frequencies of ferryl oxo hemeprotein intermediates

Heme protein	$\nu(Fe^{IV}=O)$ (cm^{-1})	$\Delta\nu(^{18}O)$ (cm^{-1})	Proximal ligand	Temperature (°C), pH	References
Cytochrome *d*	815	−46	Unknown	5, 7.5	[105]
CCO	804	−39	His	5, 7.4	[106]
Ferryl Mb	797	−26	His	20, 8.5	[107]
HRP-II (isozyme A)	789	−33	$His^{\delta-}$	RT, 11	[108]
HRP-II (isozyme A)	775, 780	−34, −35	$His^{\delta-}$	RT, 7	[108,109]
HRP-II (isozyme C)	787	−34	$His^{\delta-}$	RT, 11	[110,111]
HRP-II (isozyme C)	774, 776	−34, −30	$His^{\delta-}$	RT, 7	[108,112]
CAT-II	786	−30	Tyr^-	4, 9	[113]
CAT-II	775	−29	Tyr^-	4, 7	[113]
MPO-II	782	−35	Unknown	5, 11	[114]
CCP-ES	767, 753	−40, −28	$His^{\delta-}$	RT, 7–11	[115,116]
TPO 1, 3	778	—	$His^{\delta-}$	Alkaline	[117]
TPO 1, 3	771	—	$His^{\delta-}$	Neutral	[117]
CCP-ES	767, 753	−40, −28	$His^{\delta-}$	RT, 7–11	[115,116]
LPO-II	745	−33	$His^{\delta-}$	RT, 6–10	[116]

3.1.1. Peroxidases

The RR spectra of HRP compound II (HRP-II) were reported by Hashimoto et al. [110,112] and Terner et al. [108,111] at almost the same time. The $\nu(Fe^{IV}=O)$ RR band of HRP-II at neutral pH was found at 774–776 cm^{-1} [108,112]. This band appears at a higher frequency in D_2O than in H_2O by 2 cm^{-1} in neutral solution. In contrast, the $\nu(Fe^{IV}=O)$ band of HRP-II in alkaline solution, which is shifted to 787 cm^{-1}, exhibits no shift in D_2O. This difference has been interpreted in terms of the presence or absence of a hydrogen bond between the oxo oxygen and an amino acid residue, probably distal histidine. The pH profile of the intensity of the $\nu(Fe^{IV}=O)$ RR band indicated the mid-point pH of the change to be 8.8 and accordingly the RR spectral change was caused by the so-called heme-linked ionization [118–120]. Interestingly, the $\nu(Fe^{IV}=O)$ RR band for isotope-labelled species revealed that the oxygen atom of the $Fe^{IV}=O$ heme is rapidly exchanged with that of bulk water of solvent at pH 7.0, but not an alkaline solution (pH 11.0) [109,111,112]. Thus when the oxo oxygen is hydrogen bonded to a surrounding amino acid residue, the oxygen atom is exchanged with bulk water. Turnip peroxidase (TPO) also exhibits a pH dependent frequency change of $\nu(Fe^{IV}=O)$ [117].

Cytochrome *c* peroxidase (CCP) is the only peroxidase whose molecular structure has been elucidated by X-ray crystallographic analysis to date. CCP reacts rapidly with H_2O_2 to give rise to an intermediate called compound ES [121], which corresponds to compound I of HRP but contains ferryloxo neutral porphyrin and a protein (Trp-191) cation radical [122,123]. The $\nu(Fe^{IV}=O)$ RR band was observed at 767 cm^{-1} [115,116]. The $\nu(Fe^{IV}=^{18}O)$ RR band was identified when $H_2{}^{18}O_2$ was used in $H_2{}^{18}O$ but not in $H_2{}^{16}O$, indicating occurrence of the oxygen exchange between the $Fe^{IV}=O$ heme and bulk water. The $\nu(Fe^{IV}=O)$ RR band was definitely more intense and of higher frequency in D_2O than in H_2O as in HRP-II, but in contrast with this its frequency was unaltered between pH 4 and 11 [115].

Myeloperoxidase (MPO) is an integral component of the antimicrobial response, owing to its ability to catalyse the formation of HOCl from Cl^- and H_2O_2. Binding of Cl^- ion to the axial position of the ferric heme iron is suggested from RR spectra [124]. The Soret band of MPO is distinctly red shifted [125] and its RR spectra [126,127] are different from those of other peroxidases. The peculiar spectroscopic properties suggest the prosthetic group of MPO to be an iron–chlorin type [124,126–130] or heme A type [131,132]. Compound II of MPO (MPO-II) was characterized by Oertling et al. [114] with optical absorption and RR spectroscopies. RR studies of MPO-II at pH 10.7 located the $\nu(Fe^{IV}=O)$ RR band at 782 cm^{-1}, which is close to that of HRP-II. Identical results were obtained for the H_2O and D_2O solutions regarding both $\nu(Fe^{IV}=^{16}O)$ and $\nu(Fe^{IV}=^{18}O)$ bands, indicating no hydrogen bonding between the oxo ligand and the surrounding protein at pH 10.7. In contrast, at pH 7 the experiments with $H_2{}^{16}O_2$ and $H_2{}^{18}O_2$ did not yield any difference in the $\nu(Fe^{IV}=O)$ frequency. Thus there is exchange of the oxo ligand with bulk water similar to HRP-II [111,112]. Despite the significant spectroscopic

differences between MPO and HRP, their Fe^{IV}=O moieties and their interactions with the surrounding proteins appear to be fairly similar to each other.

Lactoperoxidase (LPO), present in mammalian milk, saliva, and tears, is involved in bacterial defence through oxidation of thiocyanate [133]. For compound II of LPO (LPO-II), the $\nu(Fe^{IV}=O)$ RR band is identified at 745 cm^{-1} [116]. This $\nu(Fe^{IV}=O)$ frequency is the lowest among the $\nu(Fe^{IV}=O)$ RR bands of heme proteins so far observed, and this may be related to the fact that its Fe^{II}–histidine stretching ($\nu(Fe^{II}$–His)) frequency at 248 cm^{-1} [134] is slightly higher than those of other peroxidases.

3.1.2. Catalase

The $\nu(Fe^{IV}=O)$ RR band was observed at 775 cm^{-1} for compound II of bovine liver catalase (CAT-II) at neutral pH [113], but was shifted to 786 cm^{-1} at alkaline pH in response to the heme linked ionization of a distal residue (probably His-74) [135]. Experiments carried out with $H_2{}^{18}O$ demonstrated that the oxo ligand of CAT-II exchanges with bulk water at neutral pH but not at alkaline pH. This aspect as well as the absolute value of $\nu(Fe^{IV}=O)$ of CAT-II bear close resemblance to those of HRP-II.

3.1.3. Cytochrome c oxidase

Cytochrome *c* oxidase (CCO) is a terminal oxidase of the respiratory chain [136,137] and catalyses dioxygen reduction coupled with cytochrome *c* oxidation and simultaneously translocates protons across the energy-transducing membrane. CCO contains two heme A groups (Fe_a and Fe_{a3}) and two copper ions (Cu_A and Cu_B) as redox active metal centres. The Fe_{a3}–Cu_B binuclear metal centre serves as a catalytic site for reduction of dioxygen. The $\nu(Fe^{IV}=O)$ RR band of CCO was reported independently around $\approx$800 cm^{-1} by Varotsis and Babcock [138], Ogura et al. [139] and Han et al. [140]. The $\nu(Fe^{IV}=O)$ bands in the latter two studies were observed to be deuterium sensitive, while it remained unchanged with D_2O in the former. Subsequently, another oxygen-isotope-sensitive band was found around 356 cm^{-1} in the same time range as the previous experients [141]. Therefore, Ogura et al. [106] carried out detailed experiments to follow the reaction with higher spectral resolution. Their results are shown in Fig. 18, where the time-resolved RR difference spectra ($^{16}O_2$ derivative minus $^{18}O_2$ derivative) observed at 1.1 ms after the start of reaction are displayed. It is clear that the band around 800 cm^{-1} consists of two bands at 804 and 785 cm^{-1} for the $^{16}O_2$ derivative and 764 and 751 cm^{-1} for the $^{18}O_2$ derivative. The 785 cm^{-1}–751 cm^{-1} pair for ^{16}O–^{18}O was shifted to 796 cm^{-1}–766 cm^{-1} in D_2O whereas the 804 cm^{-1}–764 cm^{-1} pair remained unshifted in D_2O as shown by spectrum B. The 785 cm^{-1}–751 cm^{-1} pair disappeared at higher temperatures as shown by spectrum C. The same experiments with $^{16}O^{18}O$ demonstrated that these bands did not arise from the O–O stretching mode. Consequently, Ogura et al. [106] reassigned the 804 cm^{-1}–764 cm^{-1} pair to $\nu(Fe^{IV}=$

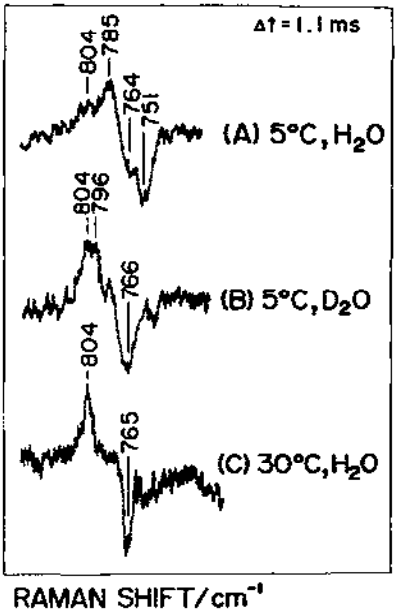

Fig. 18. Time-resolved RR difference spectra ($^{16}O_2$–$^{18}O_2$) in the ≈800 cm^{-1} region of cytochrome *c* oxidase at $\Delta t = 1.1$ ms: spectrum A, 5°C in H_2O; spectrum B, 5°C in D_2O; spectrum C, 30°C in H_2O. Resolution, 0.43 cm^{-1} channel^{-1} (450 points plotted); accumulation time, 14 220 s, 2700 s, and 540 s for spectra A, B, and C respectively. (Reproduced from ref. 106 with permission.)

^{16}O)–ν(Fe^{IV}=^{18}O) of the ferryloxo intermediate and the 785 cm^{-1}–751 cm^{-1} pair to ν(Fe^{III}–^{16}O)–ν(Fe^{III}–^{18}O) of the ferric hydroperoxy intermediate. A vibrational analysis of the FeOOH unit indicated an extremely weak O–O bond with ν(O–O) ≈ 560 cm^{-1}. The species responsible for the band at 356 cm^{-1} may be another intermediate, which has not yet been fully characterized.

3.1.4. Myoglobin

Myoglobin (Mb) is a protein for oxygen storage and reversibly binds dioxygen in the ferrous state. However, it has been known for many years that ferric Mb can react with H_2O_2 in the pH range 8–9 to yield an Fe^{IV}=O heme similar to compound II of peroxidases [142,143]. The ν(Fe^{IV}=O) RR band of ferryl Mb was found at 797 cm^{-1} by Sitter et al. [107].

3.1.5. Iron–chlorin chromophore proteins

The terminal oxidase of *E. coli* contains heme D, which corresponds to iron–chlorin, and catalyses dioxygen reduction coupled with ubiquinol oxidation. Because of a reduction of the porphyrin ring, absorption bands are red shifted and a reaction intermediate of this enzyme with O_2 gives an absorption band at 680 nm. When Raman scattering was excited at 647.1 nm for this intermediate, an oxygen-

isotope-sensitive band was observed at 815 cm^{-1} and 769 cm^{-1} for $^{16}O_2$ and $^{18}O_2$ respectively [105]. This frequency is higher than any other protein $\nu(Fe^{IV}=O)$ frequencies and its ^{16}O–^{18}O isotopic frequency shift (46 cm^{-1}) is the largest among all the ferryloxo compounds reported; 36 cm^{-1} is expected for a simple Fe=O diatomic oscillator with $\nu(Fe^{IV}=O) = 815\ cm^{-1}$. Therefore, Loehr and co-workers [105] explored the possibility that the band arose from the O^-–O^- stretching mode and examined RR spectra by using $^{16}O^{18}O$. They found no new band between the two frequencies, and therefore they assigned the 815 cm^{-1} band to $\nu(Fe^{IV}=O)$. The inordinately large isotopic frequency shift remains to be explained satisfactorily. This peculiarity was tentatively ascribed to the influence of the trans ligand, reduced macrocycle, and the lack of hydrogen bonding to the oxo ligand [105]. However, the $\nu(Fe^{IV}=O)$ RR band of iron–tetramesitylchlorin was found at 845 cm^{-1} for the five-coordinate state and at 818 cm^{-1} for the six-coordinate state with *N*-MeIm as the trans ligand [144]. Since these frequencies are almost the same as those of $(TMP)Fe^{IV}=O$ complexes, the effects of the macrocycle on the $\nu(Fe^{IV}=O)$ frequency are probably not significant.

3.1.6. Trans ligand effects on $\nu(Fe^{IV}=O)$ frequency in heme proteins

Table 5 summarizes the $\nu(Fe^{IV}=O)$ values of heme proteins so far reported. These frequencies are substantially lower than those of model compounds listed in Table 1. Factors which may cause the low frequency include trans ligand strength, local polarizability in the protein pocket, and interactions with distal residues (e.g. hydrogen bonding). Oertling et al. [22] pointed out a correlation between the $\nu(Fe^{II}$–His) and $\nu(Fe^{IV}=O)$ frequencies for several histidine-coordinated heme proteins. Ideally, the $\nu(Fe^{IV}$–His) frequencies, which are expected to be higher than $\nu(Fe^{II}$–His) frequencies, should be correlated with the $\nu(Fe^{IV}=O)$ frequencies, but unfortunately the Fe–His stretching band has never been identified for six-coordinate heme proteins or model compounds. Since the $\nu(Fe^{II}$–His) RR band is clearly observed for five-coordinate ferrous heme proteins [115,145–149] and model compounds [150,151], it can be used as a measure of the strength of this axial ligand. The $\nu(Fe^{II}$–His) frequencies are generally higher for peroxidases than for oxygen carriers owing to strong hydrogen bonding to proximal histidine. The stronger His ligation in HRP compared with Mb in the ferric state is also suggested from an extended X-ray absorption fine structure study [152]. The $\nu(Fe^{IV}=O)$ *vs.* $\nu(Fe^{II}$–His) correlation [22] indicated that the $Fe^{IV}=O$ bond becomes weaker as the Fe^{II}–His bond becomes stronger. Thus, the trans influence of the proximal ligand may enable one to modify functions of hemeproteins by replacing this residue through site-directed mutagenesis [153].

A much lower $\nu(Fe^{IV}=O)$ frequency might have been expected for CAT-II with tyrosinate as a trans ligand than for HRP-II. The reasons why it is not so are presumed to be as follows [113]. First, the proximal histidine of HRP has substantial imidazolate character owing to hydrogen bonding [151] and therefore its ligand

field strength is stronger than that of the corresponding neutral imidazole. Second, according to the X-ray crystallographic analysis of catalase [135] the phenolate oxygen of the Tyr-357 proximal ligand forms two hydrogen bonds with Arg 353 and therefore its charge density is significantly reduced [154].

3.2. *Ferryloxo porphyrin π cation radical intermediates*

Reaction intermediates which contain ferryloxo π cation radicals include compound I of HRP (HRP-I), catalase (CAT-I), chloroperoxidase (CPO-I) and the presumptive oxygen-donating intermediate of cytochrome P-450. In order to overcome their photo- and/or thermal instabilities, many different techniques, including continuous vs. pulsed lasers, visible vs. UV excitation, and spinning cell vs. continuous flowing or microdroplet stream, were adopted to determine their RR spectra. Nonetheless, RR spectra of compound I have not in general been in agreement. Their historical vicissitudes and the current situation are explained below.

3.2.1. *Horseradish peroxidase*

The RR spectrum of HRP-I was initially reported using cryogenic techniques [155], but later the spectrum was ascribed to that of ferrous HRP generated by photoreduction of HRP-I [156]. Hence Oertling and Babcock [157] adopted an alternative excitation technique to flowing samples of HRP-I and obtained a different spectrum. The key to this method is that fresh HRP-I molecules come into the scattering volume of each laser pulse with 10 ns width, and therefore the true RR spectrum would be observed if the rate of photoreduction is slower than 10 ns. However, the power density in their laser pulse was ca. 10^7-fold higher than that used for the other two measurements although the average powers were similar; the possibility that the spectrum of a photoreduced species was observed could not be completely ruled out.

It is quite important to monitor the molecules in the laser beam in order to identify the species which gives an RR spectrum. Ogura and Kitagawa [158,159] constructed a device for measuring the visible absorption and Raman spectra of molecules in the scattering volume simultaneously. Figures 19(a) and 19(b) show the simultaneously observed RR and absorption spectra respectively of resting HRP, HRP-I, and HRP-II in the flowing stream. Although the relative intensities of the ν_4 band around 1375 cm^{-1} and three other bands (ν_{10} = 1632 cm^{-1}, ν_2 = 1575 cm^{-1}, and ν_3 = 1503 cm^{-1}) are different for HRP-I and HRP-II, their frequencies are much closer than expected from the Fe^{IV}=O porphyrin π cation radicals [55]. The similarity in RR spectra between HRP-I and HRP-II, although unexpected, was ascribed to delocalization of the electron hole of the porphyrin ring to the proximal histidinate and oxygen. On the contrary, Oertling and Babcock [160] applied the pulse laser technique with flowing sample and obtained a similar spectrum but attributed it to a photo-induced reversible electron migration between the porphyrin π cation and

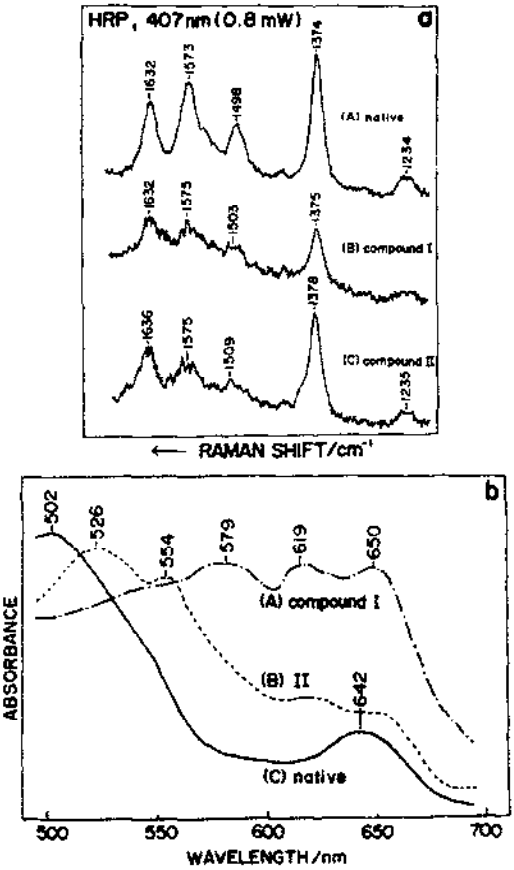

Fig. 19. (a) RR spectra and (b) absorption spectra of HRP obtained simultaneously: (a) spectrum A, and (b) spectrum C, native ferric state, 200 μM; (a) spectrum B, and (b) spectrum A, HRP-I, 100 μM; (a) spectrum C, and (b) spectrum B, HRP-II, 50 μM. HRP-I and HRP-II were obtained by mixing equal volumes of the 200 μM native enzyme with 550 μM H_2O_2 solutions, and the 100 μM HRP-I with 100 μM ferrocyanide solutions respectively. Flow rates, 0 cm s^{-1}, 8.3 cm s^{-1} and 8.3 cm s^{-1} for HRP, HRP-I and HRP-II respectively. Since the diameter of the probe beam was 0.5 mm in this experiment, the residence time of a given molecule in the laser beam was as long as 6 ms. Instrumental conditions: accumulation times for Raman spectra, 300 s for (a) spectrum A, 105 s for (a) spectrum B and 109 s for (a) spectrum C; spectral slit width, 7 cm^{-1}; relative ordinate full scales for absorption spectra are 1 (spectrum C), 0.5 (spectrum A) and 0.25 (spectrum B). (Reproduced from ref. 159 with permission.)

other moieties. Since the absorption spectrum of the sample after the Raman measurements was similar to that of HRP-I, it may be concluded that the enzyme returned to HRP-I after exposure to the laser beam.

Paeng and Kincaid [161] generated HRP-I by mixing the resting enzyme and H_2O_2 with high velocity streams of droplets. This technique shortened the residence time of the sample molecules in the laser beam (≈ 3 μs) by a factor of ≈ 1000 over that of Ogura and Kitagawa's experiment. The RR spectrum observed was quite

different from that of Fig. 19(a, spectrum B); $\Delta\nu_2 = -15\ cm^{-1}$, $\Delta\nu_3 = -7\ cm^{-1}$, and $\Delta\nu_4 = -10\ cm^{-1}$ compared with those of HRP-II. They characterized HRP-I as "a_{2u} like". They also observed the oxygen-isotope-sensitive band at 737 cm^{-1} and assigned it to the $\nu(Fe^{IV}=O)$ band of HRP-I for the first time. However, attempts by Paeng and Kincaid to repeat the droplet experiment, either in their laboratory or at the laboratory of Ogura and Kitagawa, have been unsuccessful.

Palaniappan and Terner [162] tuned the excitation wavelength to the UV, away from the strong Soret bands of HRP-II and resting HRP, and used the sample flowing technique. They observed the ν_4 band at the same frequency as that of ferrous HRP similar to the earlier cryogenic measurement [155] and revealed upshifts for ν_2, ν_{11} and ν_{37} bands with the primary contribution from the $C_\beta C_\beta$ stretching and downshifts for ν_3, ν_{10}, and ν_{28} bands with the primary contribution from the $C_\alpha C_m$ stretching. In contrast with Paeng and Kincaid [161], these frequency shifts are compatible with those of the a_{1u}-type porphyrin π cation radicals as previously described.

More recently, Chuang and Van Wart [163] reexamined the RR spectrum of HRP-I, using a rapid mixed droplet stream similar to that of Paeng and Kincaid. The frequencies of some marker bands of HRP-I reported so far are listed in Table 6. The frequencies of Raman bands, reported by Chuang and Van Wart, were different from those of Paeng and Kincaid but were rather close to those of Ogura and Kitagawa shown in Fig. 19(a, spectrum B). The spectral patterns were closer to those of Paeng and Kincaid and indicative of an a_{2u}-type radical. However, the magnitudes of the frequency shifts, which were smaller than those observed for model compounds, were attributed to delocalization of the electron hole to the axial ligands. Thus, there is a consensus among all Raman data that HRP-I is different from the porphyrin π cation model compounds so far reported; the classification of the type porphyrin π cation for HRP-I remains a vexing problem.

TABLE 6

Comparison of frequencies of some RR bands reported for horseradish peroxidase compound I generated at neutral pH

Mode[a]	Frequencies (cm^{-1}) reported in the following references			
	[159]	[161]	[162]	[163]
ν_2	1575 (—)	1569 (−15)	1606 (+19)	1575 (−12)
ν_{11}	— (—)	1545 (−17)	1570 (+10)	1552 (−8)
ν_3	1503 (−6)	1502 (−7)	1504 (−5)	1505 (−5)
ν_4	1375 (−3)	1369 (−10)	1359 (−20)	1373–6 (−3)
$\nu(Fe^{IV}=O)$	— (—)	737 (—)	— (—)	721 (−55)

[a] Frequency differences between HRP-I and HRP-II are given in parentheses.

3.2.2. Catalase

Chuang and Van Wart [163] reported the RR spectrum of CAT-I of bovine liver. Similar to HRP-I, CAT-I exhibited frequency shifts of the a_{2u} type and the frequency shifts were smaller than those of the model compounds. In contrast to HRP-I, some internal vibrations of the axial ligands (tyrosinate) were observed on excitation at 406.7 nm (1618, 1450, 1245, and 598 cm^{-1}), although the $\nu(Fe^{IV}=O)$ band was not detected. These researchers deduced that the tyrosinate$\rightarrow Fe^{IV}$ CT character is mixed with the Soret band or the radical character of the porphyrin is significantly delocalized to the tyrosinate ligand.

3.2.3. Cytochrome P-450 and chloroperoxidase

Cytochrome P-450 (P-450) is a generic name for heme proteins that exhibit a catalytic activity as a monooxygenase for a variety of organic compounds, and display a characteristic absorption band around 450 nm for their ferrous CO adducts [88]. In their catalytic reaction one oxygen atom of dioxygen is converted to water and the other is incorporated into an organic substrate. Chloroperoxidase (CPO) catalyzes the H_2O_2-dependent formation of a carbon–halogen bond in the presence of halogen anions and an organic substrate such as β-diketone [164]. The characteristic structural feature of the active sites of both enzymes is the coordination of the cysteinate sulphur anion to the heme iron [165–167]. Despite the similarities in physicochemical properties of P-450 and CPO such as the Fe^{III}–S^- bond lengths [168] and the Fe^{III}–S^- stretching frequencies [169], their reactivities are distinct.

Egawa et al. [170] applied the mixed flow transient Raman apparatus to the reaction of CPO with H_2O_2 and the results are illustrated in Fig. 20. Spectra B and C were obtained for compound I derived from $H_2{}^{16}O_2$ and $H_2{}^{18}O_2$ respectively; trace D shows their difference; spectrum D = 2 × (spectrum B − spectrum C). The formation of compound I was confirmed by simultaneously observing the visible absorption spectrum. Spectrum D exhibits a derivative-like pattern around 800 cm^{-1}, meaning that the band at 790 cm^{-1} in spectrum B is shifted to 756 cm^{-1} in spectrum C. The observed shift (34 cm^{-1}) is in excellent agreement with the theoretical value (35 cm^{-1}) expected for an isolated Fe=O diatomic oscillator. Therefore, the 790 cm^{-1} band of spectrum B was assigned to the $\nu(Fe^{IV}=O)$ band of CPO-I. The ν_4 band of resting CPO appears at 1372 cm^{-1} as shown by spectrum A but the corresponding band of CPO-I was too weak to be identified. This feature is consistent with the general property of porphyrin π cation radicals, and distinct from compound ES of CCP which gives an intense ν_4 RR band at 1378 cm^{-1} [115] owing to the formation of Fe^{IV}=O neutral porphyrin and a protein cation radical. Spectra E and F in Fig. 20 were observed for CPO-II derived from $H_2{}^{16}O_2$ and $H_2{}^{18}O_2$ respectively, and spectrum G depicts their expanded difference; spectrum G = 4 × (spectrum E − spectrum F). An oxygen-isotope-sensitive band was not recognized for CPO-II. Since spectrum E in the 1570–1650 cm^{-1} region is distinct from spectrum A, the occurrence of photoreduction during the Raman measurements is unlikely. It is highly plausible

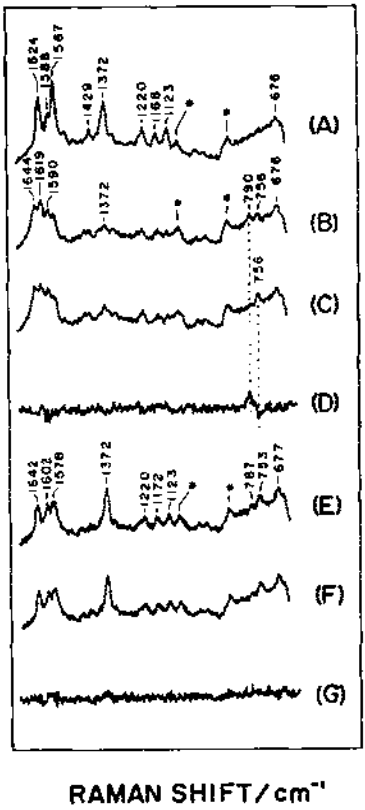

Fig. 20. RR spectra of chloroperoxidase excited at 363.8 nm: spectrum A, resting CPO; spectrum B, compound I derived from $H_2{}^{16}O_2$; spectrum C, compound I derived from $H_2{}^{18}O_2$; spectrum D, difference spectrum, 2 × (spectrum B − spectrum C); spectrum E, compound II derived from $H_2{}^{16}O_2$; spectrum F, compound II derived from $H_2{}^{18}O_2$; spectrum G, difference spectrum, 4 × (spectrum E − spectrum F). *, Raman bands of buffer solution. (Reproduced from ref. 170 with permission.)

that the Fe^{IV}=O oxygen is exchanged with bulk water as noted for HRP-II at neutral pH.

Egawa et al. [171] also pursued the reaction process of *Pseudomonas putida* P-450 (P-450_{cam}) in the presence of various reactants, such as D-camphor, β-NADH, putidaredoxin, and putidaredoxin reductase by using the mixed flow transient Raman apparatus. In its catalytic reaction the ferryloxo π cation radical was postulated to follow the ferrous oxy form. Although the dioxygen stretching RR band was identified at 1141 cm^{-1} for the ferrous oxygenated form, no other oxygen-isotope-sensitive band was detected around 800 cm^{-1} during its decay process. Lack of the ν(Fe^{IV}=O) RR band implies either that the lifetime of the ferryloxo π cation radical is extremely short or that the absorption band of the active species is located far from the excitation wavelength (420 nm).

Champion [172] proposed another scenario for the active intermediate of

Scheme I

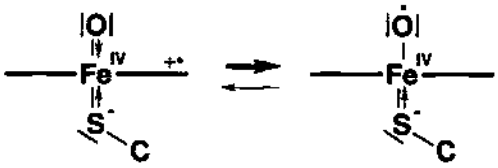

1 2

P-450 as illustrated in Scheme 1, in which an oxygen radical (**2**) instead of the compound I like structure (**1**) is formed. The relative stability between the two intermediates was thought to depend on the polarity of the heme pocket. The X-ray analysis reveals that the heme pocket of P-450$_{cam}$ is non-polar [167] and therefore structure **2** with a smaller electric dipole moment would be expected. In contrast, the heme pocket of CPO is more polar [173] and so the ferryloxo porphyrin π cation radical (**1**) is the favoured intermediate. If this proposal is correct, the Fe–O stretching frequency of the oxygen radical would be much lower than the $\nu(Fe^{IV}=O)$ frequencies of the compound I like structure. Thus, RR observation of the Fe–O stretching frequency is desirable to determine the validity of structure **2** as an intermediate of P-450.

4. CONCLUSIONS AND PERSPECTIVES

In this paper we provided a comprehensive survey on the RR spectra of highly oxidized porphyrins and heme proteins with emphasis on a few key bands. The past decade was a period for starting up of the RR characterization of highly oxidized intermediates. A sufficient amount of data have been accumulated for the key bands of the heme proteins as well as their model compounds. The present decade should be dedicated to correlating quantitatively the RR data with molecular structures, electronic structures, and reactivities. Although the RR spectra of some photolabile intermediates have not yet been established, it became apparent that the RR spectroscopic approach provides deep structural insight into unstable reaction intermediates of heme proteins and their model compounds.

ACKNOWLEDGMENTS

The authors wish to express their gratitude to Professor Paul Stein of Duquesne University for his stimulating discussion and reading of this paper during his stay at IMS. They are indebted to the work of their collaborators, the late Dr. Yoshitaka Tatsuno, Drs. Shinji Hashimoto (Tohoku University), Tsuyoshi Egawa (Keio University), Yoshihito Watanabe (Kyoto University), Takashi Ogura (IMS) and Satoru Nakashima (IMS). This study was supported in part by Grants-in-Aids of

the Ministry of Education, Science, and Culture, Japan for Priority Areas (bioinorganic chemistry) to T.K. (04225106) and for Scientific Research to Y.M. (0766).

REFERENCES

1 T.G. Spiro (Ed.), Biological Application of Raman Spectroscopy, Vol. 3, Wiley, New York, 1988.
2 T. Kitagawa and Y. Ozaki, Struct. Bonding, 64 (1987) 71.
3 T.G. Spiro, Adv. Protein Chem., 37 (1985) 111.
4 T.G. Spiro, R.S. Czernuszewicz and X.-Y. Li, Coord. Chem. Rev., 100 (1990) 541.
5 T. Yamamoto, G. Palmer, D. Gill, I.T. Salmeen and L. Rimai, J. Biol. Chem., 248 (1973) 5211.
6 T.G. Spiro and T.C. Strekas, J. Am. Chem. Soc., 96 (1974) 338.
7 T. Kitagawa, T. Iizuka, Y. Kyogoku and M.I. Saito, J. Am. Chem. Soc., 98 (1976) 5169.
8 T.G. Spiro and J.M. Burke, J. Am. Chem. Soc., 98 (1976) 5482.
9 L.D. Spaulding, C.C. Chang, N.-T. Yu and R.H. Felton, J. Am. Chem. Soc., 97 (1975) 2517.
10 A. Lanir and N.-T. Yu, J. Biol. Chem., 254 (1979) 5882.
11 T.G. Spiro, J.D. Stong and P. Stein, J. Am. Chem. Soc., 101 (1979) 2648.
12 T. Kitagawa, in R.J.H. Clark and R.E. Hester (Eds.), Raman Spectroscopy of Biological Systems, Wiley, Chichester, 1986, p. 443.
13 T. Kitagawa and T. Ogura, in R.J.H. Clark and R.E. Hester (Eds.), Biomolecular Spectroscopy, Part B, Wiley, Chichester, 1993, p. 139.
14 K. Bajdor and K. Nakamoto, J. Am. Chem. Soc., 106 (1984) 3045.
15 L.M. Proniewicz, K. Bajdor and K. Nakamoto, J. Phys. Chem., 90 (1986) 1760.
16 J.M. Burke, J.R. Kincaid and T.G. Spiro, J. Am. Chem. Soc., 100 (1978) 6077.
17 S. Hashimoto, Y. Tatsuno and T. Kitagawa, in W.L. Peticolas and B. Hudson (Eds.), Proceedings of the Tenth International Conference on Raman Spectroscopy, University Printing Department, University of Oregon, Eugene, OR, 1986, p. 1–28.
18 M. Schappacher, G. Chottard and R. Weiss, J. Chem. Soc., Chem. Commun., (1986) 93.
19 R.T. Kean, W.A. Oertling and G.T. Babcock, J. Am. Chem. Soc., 109 (1987) 2185.
20 A. Gold, K. Jayaraj, P. Doppelt, R. Weiss, G. Chottard, E. Bill, X. Ding and A.X. Trautwein, J. Am. Chem. Soc., 110 (1988) 5756.
21 Y. Mizutani, S. Hashimoto, Y. Tatsuno and T. Kitagawa, J. Am. Chem. Soc., 112 (1990) 6809.
22 W.A. Oertling, R.T. Kean, R. Wever and G.T. Babcock, Inorg. Chem., 29 (1990) 2633.
23 R.S. Czernuszewicz and K.A. Macor, J. Raman Spectrosc., 19 (1988) 553.
24 I.R. Paeng, H. Shiwaku and K. Nakamoto, J. Am. Chem. Soc., 110 (1988) 1995.
25 S.M. Chen and Y.O. Su, J. Chem., Soc., Chem. Commun., (1990) 491.
26 L.M. Proniewicz, I.R. Paeng and K. Nakamoto, J. Am. Chem. Soc., 113 (1991) 3294.
27 I.R. Paeng and K. Nakamoto, J. Am. Chem. Soc., 112 (1990) 3289.
28 Y.O. Su, R.S. Czernuszewicz, L.A. Miller and T.G. Spiro, J. Am. Chem. Soc., 110 (1988) 4150.
29 U. Mayer, V. Gutmann and W. Gerger, Monatsh. Chem., 106 (1975) 1235.
30 V. Gutmann, Electrochim. Acta, 21 (1976) 661.
31 V. Gutmann, The Donor–Acceptor Approach to Molecular Interactions, Plenum, New York, 1978.
32 R.C. Pettersen and L.E. Alexander, J. Am. Chem. Soc., 90 (1968) 3873.
33 A.L. Balch, Y.-W. Chan, R.-J. Cheng, G.N. La Mar, L. Latos-Grazynski and M.W. Renner, J. Am. Chem. Soc., 106 (1984) 7779.

34 J.T. Groves, W.J. Kruper, Jr., R.C. Haushalter and W.M. Butler, Inorg. Chem., 21 (1982) 1363.
35 R.S. Czernuszewicz, Y.O. Su, M.K. Stern, K.A. Macor, D. Kim, J.T. Groves and T.G. Spiro, J. Am. Chem. Soc., 110 (1988) 4158.
36 J. Sun and P. Stein, in J.R. Durig and J.F. Sullivan (Eds.), Proceedings of the Twelfth International Conference on Raman Spectroscopy, Wiley, New York, 1990, p. 584.
37 J. Terner and J. Topich, Chem. Phys. Lett., 106 (1984) 508.
38 T.J. Collins, R.D. Powell, C. Slebodnick and E.S. Uffelman, J. Am. Chem. Soc., 112 (1990) 899.
39 K. Yamaguchi, Y. Watanabe and I. Morishima, J. Chem. Soc., Chem. Commun., (1992) 1721.
40 M. Gouterman, in D. Dolphin (Ed.), The Porphyrins, Vol. 3, Academic Press, New York, 1978, Chapter 1.
41 H. Kashiwagi and S. Obara, Int. J. Quantum Chem., 20 (1981) 843.
42 D. Dolphin, A. Forman, D.C. Borg, J. Fajer and R.H. Felton, Proc. Natl. Acad. Sci. USA, 68 (1971) 614.
43 D. Dolphin and R.H. Felton, Acc. Chem. Res., 7 (1974) 26.
44 R. Rutter, M. Valentine, M.P. Hendrich, L.P. Hager and P.G. Debrunner, Biochemistry, 22 (1986) 4769.
45 I. Morishima, Y. Takamuki and Y. Shiro, J. Am. Chem. Soc., 106 (1984) 7666.
46 G.M. Godziela and H.M. Goff, J. Am. Chem. Soc., 108 (1986) 2237.
47 P.O. Sandusky, A. Salehi, C.K. Chang and G.T. Babcock, J. Am. Chem. Soc., 111 (1989) 6437.
48 W.A. Oertling, A. Salehi, C.K. Chang and G.T. Babcock, J. Phys. Chem., 93 (1989) 1311.
49 R.S. Czernuszewicz, K.A. Macor, X.-Y. Li, J.R. Kincaid and T.G. Spiro, J. Am. Chem. Soc., 111 (1989) 3860.
50 H. Yamaguchi, M. Nakano and K. Itoh, Chem. Lett., (1982) 1397.
51 D. Kim, L.A. Miller, G. Rakhit and T.G. Spiro, J. Phys. Chem., 90 (1986) 3320.
52 A. Salehi, W.A. Oertling, G.T. Babcock and C.K. Chang, J. Am. Chem. Soc., 108 (1986) 5630.
53 W.A. Oertling, A. Salehi, C.K. Chang and G.T. Babcock, J. Phys. Chem., 91 (1987) 3114.
54 W.A. Oertling, A. Salehi, Y.C. Chung, G.E. Leroi, C.K. Chang and G.T. Babcock, J. Phys. Chem., 91 (1987) 5887.
55 S. Hashimoto, Y. Mizutani, Y. Tatsuno and T. Kitagawa, J. Am. Chem. Soc., 113 (1991) 6542.
56 A. Salehi, W.A. Oertling, G.T. Babcock and C.K. Chang, Inorg. Chem., 26 (1987) 4296.
57 P. Gans, G. Buisson, E. Duée, J.-C. Marchon, B.S. Erler, W.F. Scholz and C.A. Reed, J. Am. Chem. Soc., 108 (1986) 1223.
58 X.-Y. Li, R.S. Czernuszewicz, J.R. Kincaid, Y.O. Su and T.G. Spiro, J. Phys. Chem., 94 (1990) 31.
59 J. Fajor, D.C. Borg, A. Forman, D. Dolphin and R.H. Felton, J. Am. Chem. Soc., 92 (1970) 3451.
60 J. Fajer and M.S. Davis, in D. Dolphin (Ed.), The Porphyrins, Vol. 4, Academic Press, New York, 1978, Chapter 4.
61 M. Huber, H. Kurreck, B. von Maltzan, M. Plato and K. Möbius, J. Chem. Soc., Faraday Trans., 86 (1990) 1087.
62 J.A. Pople and D.L. Beveridge, J. Phys. Chem., 49 (1968) 4725.
63 H. Song, C.A. Reed and W.R. Scheidt, J. Am. Chem. Soc., 111 (1989) 6865.
64 M. Abe, T. Kitagawa and Y. Kyogoku, J. Chem. Phys., 69 (1978) 4526.

65 X.-Y. Li, R.S. Czernuszewicz, J.R. Kincaid, P. Stein and T.G. Spiro, J. Phys. Chem., 94 (1990) 47.
66 D. Dolphin, Z. Muljiani, K. Rousseau, D.C. Borg, J. Fajor and R.H. Felton, Ann. NY Acad. Sci., 206 (1973) 177.
67 K. Yamaguchi, H. Fujii and I. Morishima, manuscript in preparation.
68 H. Fujii and K. Ichikawa, Inorg. Chem., 31 (1992) 1110.
69 L.K. Hanson, C.K. Chang, M.S. Davis and J. Fajer, J. Am. Chem. Soc., 103 (1981) 663.
70 K.A. Macor, R.S. Czernuszewicz and T.G. Spiro, Inorg. Chem., 29 (1990) 1996.
71 Y. Tokita, K. Yamaguchi, Y. Watanabe and I. Morishima, Inorg. Chem. 32 (1993) 329.
72 J.T. Groves, R.C. Hansbalter, M. Nakamura, T.E. Nemo and B.J. Evans, J. Am. Chem. Soc., 103 (1981) 2884.
73 S. Hashimoto, Y. Tatsuno and T. Kitagawa, J. Am. Chem. Soc., 109 (1987) 8096.
74 J.R. Kincaid, A.J. Schneider and K.-J. Paeng, J. Am. Chem. Soc., 111 (1989) 735.
75 V. Fidler, T. Ogura, S. Sato, K. Aoyagi and T. Kitagawa, Bull. Chem. Soc. Jpn., 64 (1991) 2315.
76 T. Ogura, V. Fidler, Y. Ozaki and T. Kitagawa, Chem. Phys. Lett., 169 (1990) 457.
77 J.T. Groves and Y. Watanabe, J. Am. Chem. Soc., 110 (1988) 8443.
78 H. Fujii, J. Am. Chem. Soc., 115 (1993) 4641.
79 E.W. Svastits, J.H. Dawson, R. Breslow and S.H. Gellman, J. Am. Chem. Soc., 107 (1985) 6427.
80 W.-D. Wagner and K. Nakamoto, J. Am. Chem. Soc., 110 (1988) 4044.
81 W.-D. Wagner and K. Nakamoto, J. Am. Chem. Soc., 111 (1989) 1590.
82 J.T. Groves, T. Takahashi and W.M. Buchler, Inorg. Chem., 22 (1983) 884.
83 J.W. Buchler, C. Dreher, K.-L. Lay and A. Raap, Z. Naturforsch., Teil B, 37 (1982) 1155.
84 J.W. Buchler, C. Dreher, K.-L. Lay, A. Raap and K. Gersonde, Inorg. Chem., 22 (1983) 879.
85 C. Champochiaro, J.A. Hofmann, Jr., and D.F. Bocian, Inorg. Chem., 24 (1985) 449.
86 M. Tsubaki, H. Hori, T. Hotta, A. Hiwatashi, Y. Ichikawa and N.-T. Yu, Biochemistry, 26 (1987) 4980.
87 F.P. Guengerich and T.L. MacDonald, Acc. Chem. Res., 17 (1984) 9.
88 T.J. McMurry and J.T. Groves, in P.R. Ortiz de Montellano (Ed.), Cytochrome P-450: Structure, Mechanism and Biochemistry, Plenum, New York, 1986.
89 M.M. Olmstead, R.-J. Cheng and A.L. Balch, Inorg. Chem., 21 (1982) 4143.
90 B. Chevrier, R. Weiss, M. Lange, J.-C. Chottard and D. Mansuy, J. Am. Chem. Soc., 103 (1981) 2899.
91 L. Latos-Grazynski, R.-J. Cheng, G.N. La Mar and A.L. Balch, J. Am. Chem. Soc., 103 (1981) 4270.
92 R. Bonnett, R.J. Ridge and E.H. Appelman, J. Chem. Soc., Chem. Commun., (1978) 310.
93 A.L. Balch, Y.-W. Chan and M.M. Olmstead, J. Am. Chem. Soc., 107 (1985) 6510.
94 A.L. Balch, Y.-W. Chan, M.M. Olmstead and M.W. Renner, J. Am. Chem. Soc., 107 (1985) 2393.
95 K. Tatsumi and R. Hoffman, Inorg. Chem., 20 (1981) 3771.
96 A. Strich and A. Veillard, Nouv. J. Chim., 7 (1983) 347.
97 K.A. Jørgensen, J. Am. Chem. Soc., 109 (1987) 698.
98 J.T. Groves and Y. Watanabe, J. Am. Chem. Soc., 108 (1986) 7836.
99 J.T. Groves and Y. Watanabe, J. Am. Chem. Soc., 110 (1988) 8443.
100 Y. Mizutani, Y. Watanabe and T. Kitagawa, J. Am. Chem. Soc., 116 (1994) 3439.
101 S.A. Asher and T.M. Schuster, Biochemistry, 18 (1979) 5377.
102 S.A. Asher, L.E. Vickery, T.M. Schuster and K. Sauer, Biochemistry, 16 (1977) 5849.
103 T. Uno, K. Hatano, T. Newa, K. Nakamura, Y. Nishimura and Y. Arata, Inorg. Chem., 30 (1991) 4322.

104 L.A. Andersson, T.M. Loehr, R.G. Thompson and S.H. Strauss, Inorg. Chem., 29 (1990) 2142.
105 M.A. Kahlow, T.M. Zuberi, R.B. Gennis and T.M. Loehr, Biochemistry, 30 (1991) 11485.
106 T. Ogura, S. Takahashi, S. Hirota, K. Shinzawa-Itoh, S. Yoshikawa and T. Kitagawa, J. Am. Chem. Soc., 115 (1993) 8527.
107 A.J. Sitter, C.M. Reczek and J. Terner, Biochim. Biophys. Acta, 828 (1985) 229.
108 A.J. Sitter, C.M. Reczek and J. Terner, J. Biol. Chem., 260 (1985) 7515.
109 S. Hashimoto, R. Nakajima, I. Yamazaki, Y. Tatsuno and T. Kitagawa, FEBS Lett., 208 (1986) 305.
110 S. Hashimoto, Y. Tatsuno and T. Kitagawa, Proc. Jpn. Acad. Ser. B, 60 (1984) 345.
111 J. Terner, A.J. Sitter and C.M. Reczek, Biochim. Biophys. Acta, 828 (1985) 73.
112 S. Hashimoto, Y. Tatsuno and T. Kitagawa, Proc. Natl. Acad. Sci. USA, 83 (1986) 2417.
113 W.-J. Chuang, J. Heldt and H.E. Van Wart, J. Biol. Chem., 264 (1989) 14209.
114 W.A. Oertling, H. Hoogland, G.T. Babcock and R. Wever, Biochemistry, 27 (1988) 5395.
115 S. Hashimoto, J. Teraoka, T. Inubushi, T. Yonetani and T. Kitagawa, J. Biol. Chem., 261 (1986) 11110.
116 C.M. Reczek, A.J. Sitter and J. Terner, J. Mol. Struct., 214 (1989) 27.
117 V. Palaniappan and J. Terner, In C.C. Reddy, C.A. Hamilton and K.M. Madyastha (Eds.), Biological Oxidation Systems, Academic Press, San Diego, CA, 1990, p. 487.
118 H.A. Harbury, J. Biol. Chem., 225 (1957) 1009.
119 H. Yamada, R. Makino and I. Yamazaki, Arch. Biochem. Biophys., 169 (1975) 344.
120 Y. Hayashi and I. Yamazaki, Arch. Biochem. Biophys., 190 (1978) 446.
121 T. Yonetani, in P.D. Boyer (Ed.), The Enzymes, Vol. 13, Academic Press, New York, 1976, p. 345.
122 T. Yonetani, H. Schleyer and A. Ehrenberg, J. Biol. Chem., 241 (1966) 3240.
123 M. Sivaraja, D.B. Goodin, M. Smith and B.M. Hoffman, Science, 245 (1989) 738.
124 M. Ikeda-Saito, P.V. Argade and D.L. Rousseau, FEBS Lett., 184 (1985) 52.
125 R. Wever and H. Plat, Biochim. Biophys. Acta, 661 (1981) 235.
126 S.S. Sibbett and J.D. Hurst, Biochemistry, 23 (1984) 3007.
127 G.T. Babcock, R.T. Ingle, W.A. Oertling, J.C. Davis, B.A. Averill, C.L. Hulse, D.J. Stufkens, B.G.J.M. Bolscher and R. Wever, Biochim. Biophys. Acta, 828 (1985) 58.
128 D.B. Morell, Y. Chang and P.S. Clezy, Biochim. Biophys. Acta, 136 (1967) 121.
129 D.G. Eglington, D. Barber, A.J. Thomson, C. Greenwood and A.W. Segal, Biochim. Biophys. Acta, 703 (1982) 187.
130 R.F. Stump, G.G. Deanin, J.M. Oliver and J.A. Shelnutt, Biophys. J., 51 (1981) 605.
131 J. Schultz and H.W. Schmukler, Biochemistry, 3 (1964) 1234.
132 N. Newton, D.B. Morell, L. Clarke and P.S. Clezy, Biochim. Biophys. Acta, 96 (1965) 476.
133 C.B. Hamon and S.J. Klebanoff, J. Exp. Med., 137 (1973) 438.
134 T. Kitagawa, S. Hashimoto, J. Teraoka, S. Nakamura, H. Yajima and T. Hosoya, Biochemistry, 22 (1983) 2788.
135 I. Fita and M.G. Rossmann, J. Mol. Biol., 185 (1985) 21.
136 M. Wikström, K. Krab and M. Saraste, Cytochrome Oxidase: A Synthesis, Academic Press, London, 1981.
137 S.I. Chan and P.M. Li, Biochemistry, 29 (1990) 1.
138 C. Varotsis and G.T. Babcock, Biochemistry, 29 (1990) 7357.
139 T. Ogura, S. Takahashi, K. Shinzawa-Itoh, S. Yoshikawa and T. Kitagawa, J. Biol. Chem., 265 (1990) 14721.
140 S. Han, Y.-C. Ching and D.L. Rousseau, Nature, 348 (1990) 89.
141 T. Ogura, S. Takahashi, K. Shinzawa-Itoh, S. Yoshikawa and T. Kitagawa, Bull. Chem. Soc. Jpn., 64 (1991) 2901.

142 P. George and D.H. Irvine, Biochem. J., 52 (1952) 511.
143 H. Theorell and A. Ehrenberg, Arch. Biochem. Biophys., 41 (1952) 442.
144 S. Ozawa, Y. Watanabe, S. Nakashima, T. Kiatagawa and I. Morishima, J. Am. Chem. Soc., 116 (1994) 634.
145 T. Kitagawa, K. Nagai and M. Tsubaki, FEBS Lett., 104 (1979) 376.
146 K. Nagai, T. Kitagawa and H. Morimoto, J. Mol. Biol., 136 (1980) 271.
147 M. Tsubaki, K. Nagai and T. Kitagawa, Biochemistry, 19 (1980) 379.
148 P.V. Argade, M. Sassaroli, D.L. Rousseau, T. Inubushi, M. Ikeda-Saito and A. Lapidot, J. Am. Chem. Soc., 106 (1984) 6593.
149 T. Ogura, K. Hon-nami, T. Oshima, S. Yoshikawa and T. Kitagawa, J. Am. Chem. Soc., 105 (1983) 7781.
150 H. Hori and T. Kitagawa, J. Am. Chem. Soc., 102 (1980) 3608.
151 J. Teraoka and T. Kitagawa, J. Biol. Chem., 256 (1981) 3969.
152 B. Chance, L. Powers, Y. Ching, T.L. Poulos, G.R. Schonbaum, I. Yamazaki and K.G. Paul, Arch. Biochem. Biophys., 235 (1984) 596.
153 S. Adachi, S. Nagano, K. Ishimori, Y. Watanabe, I. Morishima, T. Egawa and T. Kitagawa, Biochemistry, 32, (1993) 241.
154 V. Thanabal, J.S. de Ropp and G.M. La Mar, J. Am. Chem. Soc., 110 (1988) 3027.
155 J. Teraoka, T. Ogura and T. Kitagawa, J. Am. Chem. Soc., 104 (1982) 7354.
156 H.E. Van Wart and J. Zimmer, J. Am. Chem. Soc., 107 (1985) 3379.
157 W.A. Oertling and G.T. Babcock, J. Am. Chem. Soc., 107 (1985) 6406.
158 T. Ogura and T. Kitagawa, J. Am. Chem. Soc., 109 (1987) 2177.
159 T. Ogura and T. Kitagawa, Rev. Sci. Instrum., 59 (1988) 1316.
160 W.A. Oertling and G.T. Babcock, Biochemistry, 27 (1988) 3331.
161 K.-J. Paeng and J.R. Kincaid, J. Am. Chem. Soc., 110 (1988) 7913.
162 V. Palaniappan and J. Terner, J. Biol. Chem., 264 (1989) 16046.
163 W.-J. Chuang and H.E. Van Wart, J. Biol. Chem., 267 (1992) 13293.
164 D.R. Morris and L.P. Hager, J. Biol. Chem., 241 (1966) 1763.
165 O. Bangcharoenpaurpong, P.M. Champion, K.S. Hall and L.P. Hager, Biochemistry, 25 (1987) 2374.
166 R.E. White and M.J. Coon, Ann. Rev. Biochem., 49 (1980) 315.
167 T.L. Poulos, B.C. Finzel, I.C. Gunsalus, G.C. Wagner and J. Kraut, J. Biol. Chem., 260 (1985) 16122.
168 S.P. Cramer, J.H. Dawson, K.O. Hodgson and L.P. Hager, J. Am. Chem. Soc., 100 (1978) 7282.
169 P.M. Champion, B.R. Stallard, G.C. Wagner and I.C. Gunsalus, J. Am. Chem. Soc., 104 (1982) 5469.
170 T. Egawa, H. Miki, T. Ogura, R. Makino, Y. Ishimura and T. Kitagawa, FEBS Lett., 305 (1992) 206.
171 T. Egawa, T. Ogura, R. Makino, Y. Ishimura and T. Kitagawa, J. Biol. Chem., 266 (1991) 10246.
172 P.M. Champion, J. Am. Chem. Soc., 111 (1989) 3433.
173 M. Sono, J.H. Dawson, K. Hall and L.P. Hager, Biochemistry, 25 (1986) 347.